TECHNICAL RESEARCH REPORT

Ripple Analysis in Ferret Primary Auditory Cortex.
I. Response Characteristics of Single Units to
Sinusoidally Rippled Spectra

by S.A. Shamma, H. Versnel,
and N. Kowalski

T.R. 94-20

ISR
INSTITUTE FOR SYSTEMS RESEARCH

1. REPORT DATE **1994**	2. REPORT TYPE	3. DATES COVERED **00-00-1994 to 00-00-1994**
4. TITLE AND SUBTITLE **Ripple Analysis in Ferret Primary Auditory Cortex. I. Response Characteristics of Single Units to Sinusoidally Rippled Spectra**		5a. CONTRACT NUMBER
		5b. GRANT NUMBER
		5c. PROGRAM ELEMENT NUMBER
6. AUTHOR(S)		5d. PROJECT NUMBER
		5e. TASK NUMBER
		5f. WORK UNIT NUMBER
7. PERFORMING ORGANIZATION NAME(S) AND ADDRESS(ES) **Department of Electrical Engineering,Institute for Systems Research,University of Maryland,College Park,MD,20742**		8. PERFORMING ORGANIZATION REPORT NUMBER
9. SPONSORING/MONITORING AGENCY NAME(S) AND ADDRESS(ES)		10. SPONSOR/MONITOR'S ACRONYM(S)
		11. SPONSOR/MONITOR'S REPORT NUMBER(S)

12. DISTRIBUTION/AVAILABILITY STATEMENT **Approved for public release; distribution unlimited**

13. SUPPLEMENTARY NOTES

14. ABSTRACT **see report**

15. SUBJECT TERMS

16. SECURITY CLASSIFICATION OF:			17. LIMITATION OF ABSTRACT	18. NUMBER OF PAGES **41**	19a. NAME OF RESPONSIBLE PERSON
a. REPORT **unclassified**	b. ABSTRACT **unclassified**	c. THIS PAGE **unclassified**			

Ripple Analysis in Ferret Primary Auditory Cortex.
I. Response Characteristics of Single Units to Sinusoidally Rippled Spectra

Shihab A. Shamma[a], Huib Versnel[b], and Nina Kowalski[c]

(a) Electrical Engineering Department, University of Maryland Institute for Advanced Computer Studies, and Institute for Systems Research. University of Maryland, College Park, MD 20742.

(b) Institute for Systems Research, University of Maryland, College Park, MD 20742.

(c) Electrical Engineering Department and Systems Research Center, University of Maryland, College Park, MD 20742.

ABSTRACT

We compared the response properties of single units to tones and sinusoidally rippled spectral stimuli in the primary auditory cortex (AI) of the barbiturate-anesthetized ferret. Using two-tone stimuli, we determined the response area of each cell and parameterized it in terms of best frequency (BF), the bandwidth of the excitatory responses at 20dB above threshold (BW20), and an asymmetry index measuring the balance of inhibition and excitation around the BF. Using frequency-modulated (FM) tones, we also determined a directional sensitivity index for the cell. Using broadband stimuli (1-20 kHz) with sinusoidally modulated spectral envelopes (ripples), we measured the response magnitude of each cell as a function of ripple frequency (Ω) and ripple phase (Φ), and then reconstructed the magnitude and phase of a ripple transfer function. Most cells (approximately 90%) were tuned to a specific ripple frequency, denoted as a *characteristic ripple frequency* (Ω_o). Most cells also exhibited a linear ripple phase as a function of Ω. The intercept of the phase function defined as the *characteristic ripple phase* (Φ_o), and is interpreted as the best ripple phase to drive the cell; the slope of the phase function reflects the location of the response area of the cell along the tonotopic axis. By inverse Fourier transforming the transfer function, we obtain the *response field* (RF) of the cell, an analogue of the response area measured with tonal stimuli. Like the response area, the RF was parametrized by the following measures: BF_{RF}, which is the location of the maximum of the RF along the tonotopic axis, Ω_o, which is roughly inversely proportional to the width of the RF, and Φ_o which reflects the asymmetry of the RF. In the ferret, Ω_o ranges from 0.2 to 3 cycles/octave, with the average of the distribution around 1.0. Φ_o, ranges over the full cycle in a Gaussian-like distribution around $0°$. For a subgroup of cells the sinusoidal modulations of the spectrum were presented both on linear and logarithmic amplitude scale. The responses were not notably different. The effect of the variations of amplitude of the sinusoidal modulation was studied. The largest effect was observed for the magnitude transfer function, which increased with amplitude and then saturated. The parameters Ω_o and Φ_o did not vary significantly with ripple amplitude. Typically, cells respond best to intermediate sound levels of the ripple stimulus, i.e., the magnitude transfer function shows a nonmonotonic dependence on overall stimulus level. The phase function and Ω_o do not depend much on level. The effects of a few nonlinearities on the responses are examined briefly. Effects of nonlinearities as threshold and saturation of the neural firing rates are examined. It is found that (non)monoticity of the rate level function of a cell could be distinguished from its ripple response characterisitics. The RF of a cell closely corresponds to the response area measured with tone stimuli. Regression analysis shows that: (A) BF_{RF} is very similar to the tonal BF; (B) Ω_o is inversely correlated to the excitatory bandwidth; (C) Φ_o is correlated to the asymmetry of the response area. Responses to rippled spectra in AI resemble closely the response properties to sinusoidal gratings in the primary visual cortex (VI). This provides a unified framework within which to interpret the functional organization of both corticies. Basic differences between the two systems, however, are also evident as the lack in AI of a substantial simple/complex distinction in the responses. It is hypothesized that AI effectively analyzes an arbitrary input spectrum into a weighted sum of ripple components of different ripple frequencies and phases. This analysis is performed locally around each BF by a two-dimensional bank of filters tuned to different Ω_o and Φ_o values. Psychophysical support and implications of this hypothesis are also discussed in relation to the perception of timbre and other auditory tasks.

INTRODUCTION

Response areas of cells along the isofrequency planes of the mammalian primary auditory cortex (AI) have recently been shown to be systematically organized with respect to two properties: their excitatory bandwidths (Schreiner and Mendelson 1990) and their asymmetry (Shamma et al. 1993). To measure the response areas, these investigations employed simple tones which can be thought of as impulse-like stimuli along the tonotopic axis, as illustrated in Fig. 1 (*A*). If cortical cells were to respond linearly, the measured response areas would reflect the "impulse responses" of the system along the tonotopic axis, and hence can be used to predict the system's responses to arbitrary spectra. Furthermore, by Fourier transforming the impulse response, one obtains the corresponding "transfer function", which represents the system's response to sinusoidally modulated spectra (Fig. 1*B*), more commonly known in the psychoacoustical literature as rippled spectra (Green 1986). Consequently, response properties measured by tonal stimuli might be equally evident from their ripple transfer function.

The suggestion that cortical cells are linear may appear at first glance to be farfetched, given threshold, saturation, and the nonmonotonic behavior often seen in their rate-level functions. Nevertheless, the ripple transfer function may still yield useful insights into the response characteristics of a cell. Just as measuring with tones a cell's bandwidth, tuning quality factor, or other linear systems response properties is considered meaningful, certain characteristics of the ripple transfer functions may also prove useful, or possibly related to the properties measured with tones. It is possible as well that nonlinearities observed with tonal stimuli are less troublesome with broadband rippled spectra, or negligible over a certain range of stimulus parameters.

An analogous situation to the above has long existed in experimental studies of auditory-nerve responses. There, nonlinearities such as threshold, saturation, two-tone suppression, and adaptation are prevalent (see review in Pickles 1986). These nonlinearities, however, did not impede measurements of transfer characteristics of auditory-nerve fibers using single tones (e.g., Kiang et al. 1965), noise stimuli (e.g., de Boer and de Jongh 1978), or acoustic clicks (e.g., Pfeiffer and Kim 1972), all implying strong linear components in the responses.

Our primary goal in this report is to measure the responses of AI cells to rippled spectra at various ripple frequencies and phases, i.e., to measure their ripple transfer functions, and the dependence of this function on the amplitude of the ripples and the overall intensity of the sound. A second objective is to compare characteristic features of these transfer functions to response properties measurable using tonal stimuli, such as the bandwidth or the asymmetry of the response area.

Such an approach has proven fruitful in analogous studies of the primary visual cortex (De Valois and De Valois 1988). There, transfer functions measured using sinusoidally modulated gratings reveal much about the functional organization of the system, and its response to more complex stimuli such as oriented bars. In auditory physiology, such stimuli have only been reported by Calhoun and Schreiner (1993). Recently, several psychoacoustical studies (Hillier 1991; Vranić-Sowers and Shamma 1994a, 1994b) have converged on the similar notion that measuring the perceptual thresholds of rippled spectra may help explain how spectral profiles are perceived. A somewhat different stimulus, called the "linear ripple" spectrum, has been used extensively to investigate the perception of pitch (Yost et al. 1978) and in physiological experiments in the dorsal cochlear nucleus (Bilsen et al. 1975). Unlike our rippled spectra

which are sinusoidal along a logarithmic frequency axis (roughly the tonotopic axis), the "linear ripple" spectra are sinusoidal along the linear frequency axis, mimicing the harmonic structure of complex sounds.

METHODS

Surgery and animal preparation

The data presented here are obtained from acute experiments in 7 young adult male ferrets *Mustela putorius* weighing approximately 1.5 kg. A detailed description of the animal preparation is given in Shamma et al. (1993). Briefly, the ferrets were anesthetized with sodium pentobarbital (40 mg/kg). An areflexic level of anesthesia was maintained throughout the experiment by continuous intravenous infusion of pentobarbital (approximately 5 mg/kg/hr) diluted with dextrose-electrolyte solution. The ectosylvian gyrus, which includes the primary auditory cortex was exposed by craniotomy and the overlying dura was incised and reflected. The brain was covered in 2% agar in saline to reduce pulsations. The contralateral meatus was exposed, cleaned and partly resected, and subsequently a cone-shaped speculum containing a Sony MDR-E464 miniature speaker was sutured to the meatal stump.

Acoustic stimuli

Two types of stimuli were used in these experiments. The first type consisted of pure tone stimuli (single and two-tone bursts, 200 ms duration, 10 ms rise- and fall-times, 50 ms intertone delay) and FM tones (2 octaves around BF, at sweeping rates 50-250 octaves/s, two sweep directions). These were generated using two independent function generators, gated and mixed, and then fed through a common equalizer into the earphone. Other parameters of the test stimuli are described in RESULTS and in Shamma et al. (1993).

The second type of stimuli were broadband complex sounds. This stimulus, schematically shown in Fig. 2, consisted of 101 tones that were equally spaced along the logarithmic frequency axis and spanning 4.32 octaves (e.g., 1-20 kHz or 0.25-5 kHz). The range was chosen such that the best frequency (BF) of the cell tested lay well within the stimulus' spectrum. The envelope of the complex was then modulated sinusoidally either on a linear or on a logarithmic amplitude scale to create the so-called ripple spectrum. In the linear case, the amplitude of the ripple was defined as the maximum percentage change in the component amplitudes (left ordinate in Fig. 2). In the logarithmic scale case, it was taken as the logarithm of the ratio of the amplitude of the highest (peak) to the lowest (valley) components in the complex (right ordinate in Fig. 2). The overall level of the complex stimulus was defined by the level of a single frequency component, L_1 dB SPL in the flat complex. Thus, the overall level for a flat complex with 101 components (ripple amplitude ΔA at zero) was taken to be $L_1 + 10 \log(101) \approx L_1 + 20$ dB. The overall level was varied over a range of 30 dB. Higher levels were avoided to ensure the linearity of our acoustic delivery system.

The ripple frequency (Ω) is measured in units of cycles/octave against the logarithmic frequency axis (see Fig. 2). The ripple phase (Φ) is measured in radians (or degrees) relative to a sinewave starting at the left edge (low frequency edge) of the complex (Fig. 2). The complex stimulus bursts had 10 ms rise/fall time and 50 ms duration. They were computer synthesized, gated, and then fed through a common equalizer into the earphone.

Calibration of the sound delivery system (up to 20 kHz) was performed in situ using a 1/8-in. Brüel & Kjaer probe microphone (type 4170). The microphone was inserted into the ear canal through the wall of the speculum to within 5 mm of the tympanic membrane. The speculum and microphone setup resembles closely that suggested by Evans (1979). See more details in Shamma et al. (1993). Maximum tone intensities used were limited to 85 dB SPL to avoid any distortion.

Recordings

Action potentials from single units were recorded using glass-insulated tungsten microelectrodes with 5-6 MΩ tip impedances. Neural signals were led through a window discriminator and the time of spike occurrence relative to stimulus delivery was stored using a Hewlett-Packard 9000/800 series minicomputer. The computer also controlled stimulus delivery, and created various raster displays and spike count histograms of the responses.

In each animal, electrode penetrations were made orthogonal to the cortical surface. An experiment consisted of about 10 useful microelectrode penetrations. In each penetration, 1-7 cells were studied, typically at depths of 350-600 μm corresponding to cortical layers III and IV where excitatory phasic responses to single tones are strongest (Shamma et al. 1993).

Data analysis for the tonal stimuli

For each cell, we first manually determined the best frequency (BF), defined as the frequency of the lowest threshold, followed by a response curve with up to 1/8 octave resolution at low intensity. The rate-level function at BF was measured in order to determine the cell's response threshold and the nonmonotonicity, i.e., whether the spike count decreased by more than 25% as intensity was increased.

Subsequently, the response area was determined using the two-tone stimulus described in detail in Shamma et al. (1993). Briefly, it consisted of two tone bursts of equal duration with staggered onset times. The first tone burst (T1) was presented at several different frequencies centered around the BF of the cell to measure the excitatory response area. Since many cells exhibit low spontaneous firing rates, a second tone burst (T2) was fixed at BF, with a 50 ms delay relative to T1, to provide a level of background activity against which the inhibitory response area could be measured. Staggered onset times for T1 and T2 were used in order to segregate the phasic responses to the two tones, which made it relatively easy to determine in the same test the borders of the excitatory responses to T1 and of the inhibitory influences upon T2 as described in Shamma et al. (1993). Note that the term "response area" is used here to denote the response of a cell as a function of a tone's frequency and intensity. In the experiments reported here, the responses were usually obtained only at two intensities (around 20 dB above the threshold at BF), thus in using the term response area reference is made only to specific slices of the area (see Shamma et al. (1993) for a fuller discussion of these response measures).

The bandwidth of the excitatory response area was determined at 20 dB above the threshold at BF, and denoted as BW20. The upper and lower frequencies were found by interpolation using a criterium of 10% of the maximum response. A correction was made for possible spontaneous activity.

Another important feature of the response area is the asymmetry of its inhibitory and excitatory portions around the BF. To quantify this feature, the following simple statistic was

introduced in Shamma et al. (1993):

$$M = \frac{R_{>BF} - R_{<BF}}{R_{>BF} + R_{<BF}}, \tag{1}$$

where $R_{>BF}$ and $R_{<BF}$ are the total number of spikes to both tones for an equal number of frequencies above and below the BF, respectively. If the excitatory and inhibitory responses are approximately symmetric around BF, the measure (M) will be near zero. Inhibition of T2 responses by T1 stimuli above BF and/or spread of T1 excitation to lower frequencies ($<$ BF) causes M to be negative. Conversely, stronger low frequency inhibition or high frequency T1 excitation produces positive M values. Note that the M index as defined above is computed at one T1 intensity. Since the two-tone test was performed at two intensities of T1, indices are computed for both intensities, and then averaged.

Finally, FM tones were presented in two sweep directions, and at different rates and at similar intensities as in the two-tone tests. The symmetry of the average responses to the two sweep directions was assessed using the index C as follows (Shamma et al. 1993):

$$C = \frac{R\downarrow - R\uparrow}{R\downarrow + R\uparrow} \tag{2}$$

where $R\uparrow$ and $R\downarrow$ are the spike counts to the up and down sweeps, respectively. The index is computed for each intensity presented, and then averaged.

Data analysis for the rippled spectrum stimuli

Following the tonal stimuli, a series of tests were carried out using rippled spectra with a range of ripple frequencies Ω (typically from 0-4 cycles/octave with different resolutions) and ripple phases Φ (from $0-7\pi/4$ in $\pi/4$ steps). Different ripple amplitudes and overall stimulus levels were also tested.

Figure 3 illustrates the display and initial analysis applied to the data. Here the cell was tested over ripple frequencies 0-2 cycles/octave in steps of 0.4 cycles/octave. In Fig. 3A, the raster shows the responses to different phases of the ripple at $\Omega = 0.8$ cycles/octave. The response spike counts were made over a 50 ms time window starting shortly (10 ms) after the onset of the stimulus as indicated by the short arrows. From each such raster, spike counts were computed showing the dependence of the response on the phase of the ripple (inset plot to the right of the raster). All spike counts reflect the total responses obtained from 20 repetitions of each stimulus. In Fig. 3B, such spike counts from all ripple frequencies are combined in one display. Note that for each ripple frequency, the baseline of the plot is set equal to the average spike count from all 8 phases.

In order to analyze the different components of the response, and specifically to estimate the level of the component synchronized to each ripple frequency, an 8-point Fourier transform is performed on the spike counts at each ripple frequency (Fig. 3C). The first column is the baseline or the DC component in the responses to each ripple (or simply the average spike count). The second column (labeled $AC_1(\Omega)$) lists the magnitude and phase of the primary response component synchronized to the ripple frequency Ω. In effect, this is the amplitude and phase of the sinusoid that best fits the data at each ripple frequency (solid lines in Fig. 3B). Higher-order harmonics of the response to each ripple are listed in the other columns.

If the cell responses were completely linear and noise-free, $AC_1(0)$ (the synchronized component to a flat spectrum) and high-order harmonics at all Ω would vanish. In that case, $AC_1(\Omega)$ is the transfer function of the cell. However, this is rarely the case. So in order to take into account the magnitude of the nonlinearity and to reduce the effects of statistical noise, a normalized measure of the $AC_1(\Omega)$ responses (called $T(\Omega)$) is defined as follows:

$$T(\Omega) = AC_1(\Omega) \cdot \frac{|AC_1(\Omega)| - |AC_1(0)|}{\sqrt{\sum_{i=1}^{4} |AC_i|^2(\Omega)}} \text{ if } |AC_1(\Omega)| - |AC_1(0)| \geq 0 \qquad (3)$$

$$T(\Omega) = 0 \text{ if } |AC_1(\Omega)| - |AC_1(0)| < 0$$

where $|AC_i(\Omega)|$ is the magnitude of the response $AC_i(\Omega)$. Thus, aside from removal of the bias $AC_1(0)$, the normalized transfer function $T(\Omega)$ de-emphasizes magnitude estimates where the high-order harmonics are comparable to the $AC_1(\Omega)$, i.e., where reponses are highly nonlinearly distorted or very noisy. Note that the normalization does not affect the phase of the responses. In general terms $T(\Omega)$ can be written as follows:

$$T(\Omega) = |T(\Omega)|e^{j\Phi(\Omega)} \qquad (4)$$

Figure 4A illustrates the magnitude $|T(\Omega)|$ and the unwrapped phase $\Phi(\Omega)$ of the transfer function $T(\Omega)$ for the cell in Fig. 3. This ripple transfer function can be inverse Fourier transformed to obtain the impulse response of the cell shown in Fig. 4B. For a linearly responding cell, this function would be identical to a slice of the response area of the cell such as measured with two-tone stimuli. However, given likely nonlinearities in the responses, the two functions will not be identical. In order to distinguish it from the response area, this impulse response will be called the response field (RF) of the cell, and thought of as analogous to a slice of the response area of the cell measured at a given tone intensity. Repeating the measurements at different ripple amplitudes, we would obtain the full RF. Furthermore, performing the measurements at different overall sound levels is similar to choosing different overall levels of the two-tone stimuli.

Since these tests take a relatively long time to conduct, it was nearly impossible to hold a single unit long enough to measure both its full response area and its RFs at several ripple amplitudes. Moreover, it was desirable to examine the RFs from a large number of cells. Consequently, to compare the RFs and response areas, the RF was characterized in terms of parameters similar to the bandwidth and asymmetry indices used to describe the response area. These and other parameters of interest here are indicated in Fig. 4A. The first is the ripple frequency (Ω_o) at which the magnitude of the transfer function, $|T(\Omega)|$, is maximum. We shall call this parameter the characteristic ripple of the cell. This parameter reflects the width of the RF near its center. In general, the higher the characteristic ripple, the narrower the corresponding RF.

Two other parameters are derived from a linear fit of the phase function according to

$$\Phi(\Omega) = x_o\Omega + \Phi_o \qquad (5)$$

where x_o is the slope of the line, and Φ_o is its intercept. The parameter x_o represents the location (in octaves) of the center of the RF relative to the left edge of the ripple (Fig. 4B). The center of

the RF is defined as the center of the envelope of the RF (dashed line in Fig. 4B); this envelope is computed from the *analytic signal* corresponding to the RF function (see Oppenheim and Schafer 1990). The parameter Φ_o shall be called the characteristic phase. It roughly reflects the asymmetry of the RF about its center. For instance, the RF is symmetric for $\Phi_o = 0$, and strongly asymmetric for $\Phi_o = \pm 90°$. This is illustrated in Fig. 4C where the RF of the cell is computed for different Φ_o's by simply sliding its fitted phase function $\Phi(\Omega)$ vertically.

The straight line fit of the phase data was done in two ways. The first was to select the reliable phase values (e.g., those for which the magnitude of $AC_1(\Omega)$ is 50% larger than the other response harmonics), and then to fit these points using regular least square error procedures. The second method was to compare the RF obtained from the transfer function, $|T(\Omega)|e^{j\Phi(\Omega)}$, to the approximate $\widehat{RF}$ obtained from the same transfer function assuming it has linear phase, i.e., $|T(\Omega)|e^{j(x_o\Omega + \Phi_o)}$. The search and comparison was performed by first selecting a Φ_o, computing the $\widehat{RF}$, and then testing different x_o values by cross correlating it with the RF. The location and value of the maximum of the correlation function indicate, respectively, the best x_o for that Φ_o and the similarity of the two RFs. This procedure was then repeated for $-\pi < \Phi_o < \pi$ at the desired resolution. The best estimates of the Φ_o and x_o are those that produce the largest correlation maximum. The primary advantage of the latter procedure is that it requires no selection of phase data. Furthermore, it produces an indicator of the reliability of the linear-phase assumption, namely the largest maximum of the correlation function normalized by the length of the two RFs (a maximum value of 1 indicates a perfect fit; 0 indicates no similarity). For instance, the phase-fit indicator for the responses in Fig. 4 is 0.99. In most cases, the two fitting procedures produce very similar results. When significantly different ($> 30°$), the first method is prefered since only reliable phase estimates are used.

Another response measure of interest is the location of the maximum of the RF along the stimulus (tonotopic) axis (BF_{RF}). This can be roughly compared to the BF of the cell, or more accurately to the maximum of a slice in the cell's response area at some appropriate intensity. In the cases where BF_{RF} changes significantly with ripple amplitude or sound intensity, the estimate from the lowest stimulus levels is selected.

In this paper three response parameters in particular are used top describe the ripple responses of AI units: the characteristic ripple frequency Ω_o the characteristic phase Φ_o and the RF's best frequency BF_{RF}.

RESULTS

The data illustrated here were collected from a total of 104 single-unit recordings in 7 animals. All these units responded to tones. For 92 of tested AI units (88 %) responses to rippled spectra were locked to the phase of the stimulus. An example of dependence on phase is shown in Fig. 3A, where for a 180° shift the response changes from maximum to minimum (zero). In this paper the responses are considered with respect to their phase-following (or vector-strength) of the ripple. The response irrespective of phase (e.g., the average rate) is only discussed in the context of nonlinear behaviour.

In this section detailed features of the responses to the rippled spectra are first described, together with their dependence on the ripple amplitude and overall sound level. Next, the correspondence between the shapes of the RFs and of the response areas is examined in general

terms, and then in specific terms using such parameters as the characteristic ripple and phase, the response area bandwidth and asymmetry indices.

Responses to rippled spectra

The two most important features of cortical cell responses to rippled spectra were: (1) they were tuned to specific ripple frequencies (a characteristic ripple Ω_o), and (2) they exhibited a constant phase delay (a characteristic phase Φ_o) plus a linear phase function of the ripple frequency. The first of these features is demonstrated in Fig. 5 for three cells that are tuned to progressively higher Ω_o's (0.6, 1.0, 1.8 cycles/octave) as seen in the $|T(\Omega)|$ plots in the left column. Inverting the transfer function $T(\Omega)$ in each case produces the corresponding RFs (shown in the right column). Cells with higher Ω_o tended to have narrower RFs. Most cells exhibited tuning to a single ripple frequency. It was common that the response curve showed multiple peaks, most often in the form of a weaker tuned response at higher ripple frequencies (e.g., see $|T(\Omega)|$ plot in Fig. 5A), and in fewer cases at a lower ripple frequency (as in Fig. 5C). A few cells had strongly tuned $DC(\Omega)$ responses relative to the phase-following responses; they are discussed later. Some cells had very weak responses (or even none) in general to rippled spectra compared to tonal stimuli.

Figure 6 illustrates the transfer functions of 3 cells with comparable characteristic ripples ($\Omega_o = 0.8$), but different characteristic phases Φ_o's. A typical feature of the phase function $\Phi(\Omega)$ is its strongly linear character over a wide range of ripple frequencies (see also Fig. 5). The slope of this phase function reflects an RF displacement along the tonotopic axis relative to the low-frequency edge of the stimulus. The linearity of $\Phi(\Omega)$ also implies that the transfer function contributes only a constant phase shift (Φ_o) to all ripple frequencies. The RFs in Fig. 6 have different asymmetries reflecting the different Φ_o's.

The distributions of characteristic ripples and phases in our sample are shown in Figs. 7A and B. The range of Ω_o is 0.2-3 cycles/octave, and the average of the distribution lies around 1.0. The distribution of Φ_o is Gaussian like with most cells (61 %) between -45 and +45. The distribution is slightly biased towards negative values. In Fig. 7C-D, scatter plots of the Ω_o and Φ_o against the BF of each unit are shown. The only apparent dependence on BF is seen for the Ω_o's where units with a lower BF tend to have smaller values. The joint distribution of these two response measures is reflected by the scatter plot in Fig. 7E. It indicates that the mean and variance of the Φ_o distribution remain relatively constant and hence independent of the Ω_o. Finally, the average width of the transfer functions $|T(\Omega)|$ against the Ω-axis (measured at the 3 dB points) is found to be 1.3 octaves (SD = 0.5).

Linear vs. logarithmic ripple spectra

It is unknown whether the central auditory system encodes the shape of the acoustic spectrum on a linear or a logarithmic amplitude scale, or via other representations such as the power spectrum. Because of this uncertainty the responses of 10 cells were measured using both linear and logarithmic ripples in order to determine whether any of the response features depended critically on this choice. There are no systematic differences between the responses to these stimuli. This is illustrated for two units in Fig. 8. Slight differences in magnitude or phase functions might show up without essentially affecting the estimate of the RF.

Dependence of the responses on ripple amplitudes

Ripple spectra were presented at various ripple amplitudes in order to assess the stability of the responses. Figure 9 illustrates typical responses measured in 2 out of a total of 10 cells so tested. In both units the transfer function was measured at three ripple amplitudes. Over an intermediate range of amplitudes, the overall scale of the magnitude transfer function increases with ripple amplitude. The phase function $\Phi(\Omega)$, and the parameters Ω_o and Φ_o, remain relatively stable with ripple amplitude. At large amplitudes (e.g., at 50% in Fig. 9A), the growth of $|T(\Omega)|$ saturates but the overall shape of the transfer function is not much affected. With decreasing amplitude, the responses gradually weaken, and the $|T(\Omega)|$ becomes more noisy before disappearing (threshold at about 1 dB or 25%).

Dependence of the responses on stimulus level

Response properties were examined with respect to a change in overall stimulus level in 35 cells. Typical responses are shown for 5 cells in Fig. 10 (2 other examples follow in the next subsection). As shown in Fig. 10A,B $|T(\Omega)|$ is optimal at medium levels and decreases at the highest level while approximately maintaining its overall shape and Ω_o. Also, $\Phi(\Omega)$ functions are stable with level. Consequently, the shape of the response field does not vary significantly with level. The nonmonotonic change of $|T(\Omega)|$ with stimulus level is further demonstrated in Fig. 10C. The responses of 3 units are shown at the characteristic ripple frequency Ω_o over a 30 dB range starting at threshold level. In two cells, an optimal stimulus level is evident within the 30 dB range. In the other, the responses grew slower with level and whether $|T(\Omega)|$ decreased at higher stimulus levels (> 65 dB) could not be confirmed. In 12 of 18 cells where we measured curves as in Fig. 10C nonmonoticity was demonstrated. The nonlinear dependence of $T(\Omega)$ on level occured both in units that had nonmonotonic (Fig. 10A) or monotonic rate-level functions for BF tones (Fig. 10B). The possible reasons for the observed nonlinear dependence of $|T(\Omega)|$ on level are explored in the next subsection.

The results can be summarized with two general observations: (1) there is only a narrow effective (or "best") range of levels (usually 20 dB) over which $T(\Omega)$ responses are large. (2) Φ_o, and to a lesser extent Ω_o, are relatively stable with stimulus level in the optimal range.

Nonlinearities in the responses

All the results so far have emphasized the linear character of the responses to ripple stimuli. However, several nonlinearities exert strong influences on the responses. Two relatively easy to describe nonlinearities are threshold and saturation. The threshold nonlinearity implies half-wave rectification of the phase- locked responses.

Figures 11 and 12 show the effects of nonlinearities on the ripple responses for cells with nonmonotonic and monotonic rate-level functions at BF tones (plots *A*), respectively. The effects of the threshold nonlinearity are most evident at the lower stimulus levels, i.e., for the 50 dB responses in both examples shown. The effects are similar for nonmonotonic and monotonic cells. For instance, the nonmonotonic cell (Fig. 11) responds to a 50 dB flat spectrum ($\Omega = 0$) at an average spike count of 1.7 ($DC(0) = 1.7$ in Fig. 11D). However, when $\Omega = 0.4$ the responses become strongly modulated by the phase of the ripple (Fig. 11B), increasing up to 12 in one half cycle, and becoming half-wave rectified in the other. This rectification creates a large $DC(\Omega)$ component which is proportional to $|T(\Omega)|$ as seen in Fig. 11D (plot at 50 dB).

Exactly the same observations apply to the 50 dB data of the monotonic cell illustrated in Fig. 12.

However, at the higher stimulus level (60 dB), the responses of the two types of cells diverge significantly. For the nonmonotonic cell, all phase-locked responses become suppressed (Fig. 11B), and hence both $|T(\Omega)|$ and $DC(\Omega)$ decrease together in amplitude (Figs. 11C and D at 60 dB). For the monotonic cell in Fig. 12, increasing the stimulus level to 60 dB drives the responses harder into saturation. Consequently, the $DC(\Omega)$ response increases with level (Fig. 12D). In contrast, the phase-modulated responses (Figs. 12B and C) decrease, and hence $|T(\Omega)|$ and $DC(\Omega)$ are inversely related. Note also that $|T(\Omega)|$ is most distorted (saturated) near Ω_o, sometimes causing the entire function to appear slightly shifted downwards (Fig. 12C).

In a few cells, the response patterns exhibited complex features that could not be fit within the data analysis framework presented so far. For instance, 4 units had a strongly tuned $DC(\Omega)$, and only weak $T(\Omega)$ responses. In 3 others, the tuned $DC(\Omega)$ responses could not be simply related to $T(\Omega)$ as was the case earlier in Figs. 11 and 12. Such a response is illustrated in Fig. 13, where the $T(\Omega)$ is tuned to a rather low $\Omega_o = 0.4$, whereas $DC(\Omega)$ is strongly tuned to a much higher and apparently unrelated ripple frequency (5 cycles/octave). Since most cells in our sample were tested over a limited ripple frequency range ($0 - 4$ cycles/octave), it is unclear whether the $DC(\Omega)$ tuning at high ripple frequencies is common.

Comparison between the RF and response area

Figure 14A compares RFs (solid lines) to response areas as derived from two-tone responses (dashed lines) for three different cells. The RFs of different asymmetries and bandwidths match closely their response area counterparts (apart from the artificial elevation of responses towards the response area edges due to the BF tone (T2) of the two-tone stimulus). A qualitatively good correspondence is found in most cells, even in cells that have atypical RFs and response areas. An example of such responses is a double-peaked excitatory tuning which is illustrated in Fig. 14B.

In order to quantify more efficiently this relationship for all units, three types of parameters were computed from the RFs and response areas, and juxtaposed in scatter plots; they reflect the BF, the bandwidth, and the asymmetry of the response areas and fields.

Comparison between the BF and the BF_{RF}

The simplest measure of the correspondence between a unit's responses from tonal and rippled stimuli is in terms of its estimated BF. This is shown in Fig. 15 as a scatter plot between the BF measured with a single tone against the maximum of the RF (BF_{RF}), compiled from all units where both parameters could be measured. Obviously, for a majority of the cells the parameters were very similar. Only for 9 % of the cells the BF measures differed by more than half of an octave.

Comparison between $BW20$ and the characteristic ripple Ω_o

Another parametric comparison between the response area and the RF of a cell is in terms of their widths. For the response area, the bandwidth is measured from the excitatory tone responses 20 dB above threshold, BW20. For the RF, we measured the width of the positive peak between the zero crossings. Figure 16A shows the scatter plot of the RF width versus

BW20. In this plot only RFs with a single dominant positive peak are included ($|\Phi_o| < 90°$). The correlation between the two plot parameters is significant ($p < 0.01$).

Since the width of the RF is only indirectly related to the parameters of the ripple transfer function, the relation of the characteristic ripple Ω_o to BW20 was directly examined. Ω_o is expected to be inversely proportional to the RF width and BW20 (Figs. 4 and 5), and this is indeed supported by the scatter plot of Fig. 16B. More precisely, for a small BW20 the best ripple varies from 0.2 to 3 cycles/octave and for broadly tuned cells (BW20 > 1.5 octave) the best ripple is smaller than 1.2 cycles/oct. Despite their considerable scatter ($r = -0.27$), these data indicate that a cell is likely to be best driven by ripples with frequencies that match the outlines of the excitatory and inhibitory fields of the response area.

It is evident from the scatter plots in Fig. 16 that Ω_o is not always a good measure of the RF width. The reason for this is illustrated in Fig. 6 where the cells have the same nominal Ω_o, but quite different widths of their RFs. This reflects the different shapes and widths of their $|T(\Omega)|$ functions. Specifically, if the $|T(\Omega)|$ spreads out considerably beyond its Ω_o (e.g., as in Fig. 6B), then the RF will be narrower than predicted exclusively by its Ω_o.

The linearity of the phase function $\Phi(\Omega)$

The phase of the transfer function was fit by a straight line whose slope (x_o) and intercept (Φ_o) were associated with the horizontal shift and asymmetry of the RF, respectively (see Fig. 4). One indicator of the accuracy of this fit is the normalized match between the RF of the cell (cf. Fig. 4B), and the reconstructed RF computed from the same transfer function assuming the phase function is linear (cf. Fig. 4C). If the two patterns are identical the indicator is 1 and if they are random the indicator is 0. As is evident in all examples in Figs. 4-10, the linear fit is accurate. In 84% of all cells responding to the ripples, the indicator exceeded 0.9. That is, in these cases, the assumption of a linear phase is justified, and the Φ_o and x_o are both meaningful measures of the RF.

Comparison between M and C asymmetry indices and the characteristic phase Φ_o

The asymmetry of the response areas and of the RFs are compared in Fig. 17A. The asymmetry of the RF is indicated by the characteristic phase Φ_o and it is plotted against the asymmetry of the response area as reflected by the M index. There is a positive correlation between the two parameters which is weak but significant ($r = 0.33$; $p < 0.01$). Furthermore, in Fig. 17B Φ_o is plotted versus the asymmetry measure obtained from FM responses, the C index. Here it is more evident that the asymmetry measures from tonal and ripple stimuli do correspond ($r = 0.42$; $p < 0.001$). For comparison, the M and C indices for the same cells are plotted against each other in Fig. 17C. The correlation between the two tonal measures is only slightly larger than that of the tone-ripple response comparison ($r = 0.46$; $p < 0.001$).

DISCUSSION

The linearity of cortical cell responses to spectral ripples

Responses of single-units in AI suggest that there is generally a good correspondence between the shape of a response area (measured with tonal stimuli) and that of the RF (measured with ripple transfer functions). Specifically, for most cells the BF_{RF} is very similar to BF

(Fig. 15), and there is a reasonable correlation between the response area bandwidth and the RF width and Ω_o (Fig. 16), and between the asymmetry of the response area and that of the RF (Fig. 17). These findings in single units are confirmed in another set of experiments with multiunit recordings (Versnel et al. 1994). The correspondences between ripple and tonal responses must imply that there is a significant linear component in the cells' responses, or that at least, the nonlinearities do not completely distort such linear response measures as the transfer function $T(\Omega)$. This conclusion is consistent with findings by Nelken et al. (1994) that responses to complex sounds (e.g., nine-tone complexes) are predictable on the basis of the response areas measured with two-tone stimuli.

However, it is also evident from the various scatter plots that, apart from the BF–BF$_{RF}$ comparison, the correlations between the tonal and ripple response parameters are noisy. Apart from various response nonlinearities, which will be discussed in more detail later, other sources may contribute to this scatter. Primary among them is the approximate nature of the response parameters. For example, while parameters such as the Ω_o and Φ_o capture efficiently the shape of of the RF, they nevertheless can vary over a certain range without causing significant distortion of the RF (e.g., as in all cases of Figs. 8-10). Thus, measurements of these and other parameters (e.g., BW20 and M index) at one or a limited range of stimulus conditions must cause significant reduction in the correlations in Figs. 15-17. Nevertheless, given these and other possible sources of measurement errors, the persistance of a significant correlation between the tonal and ripple response measures is a testimony to the robustness of the linear component in the responses.

Functional significance of the response characteristics

The vast majority of units encountered in AI exhibited tuned responses as a function of ripple frequency, i.e., had a well defined characteristic ripple. Furthermore, the characteristic ripples spanned a range of frequencies (0.2 - 3 cycles/octave), and were not simply clustered around one value (Fig. 7A). These findings suggest that AI cells can in principle function as ripple bandpass filters, analyzing an input spectral profile into seperate channels tuned around different characteristic ripple frequencies. Equivalently, from the perspective of their response area bandwidths, they can be said to have a range of bandwidths so as to analyze the input spectral profile into different scales. Thus, cells with broader bandwidths respond best to the gross (slowly varying) features of the profile, whereas narrowly tuned units detect the fine (rapidly varying) features of the profile. The validity of this functional view is strengthened by the psychoacoustical findings discussed later in this section, and by the physiological mappings demonstrating a spatially organized distribution of this response property across the surface of AI (Schreiner and Mendelson 1990; Heil et al. 1992; Versnel et al. 1994).

The second important property of AI responses is the linearity of their phase functions $\Phi(\Omega)$. This implies that, apart from a linear phase shift due to the RF location relative to the left edge of the ripple stimulus (cf. Fig. 4B), the transfer function $T(\Omega)$ of an AI cell has a constant phase Φ_o. The functional interpretation of this finding is that a unit is selective not only to a characteristic ripple frequency (Ω_o), but also to a particular (characteristic) phase Φ_o of that ripple. In this sense, AI cells analyze the input spectral profile into yet another dimension, namely the phase of the ripples. This interpretation is consistent with findings that AI cells with asymmetric response areas are selectively responsive to spectral profiles with the opposite asymmetry (Shamma et al. 1993; Vranić et al. 1993), since the characteristic phase

is correlated with the asymmetry of the response area (Fig. 17).

There are, however, two important constraints on the above ripple analysis model. The first is that the distributions of the Ω_o and Φ_o are are not uniform. Instead, Ω_o in the ferret is largely limited below 2 cycles/octave, while Φ_o is dominant around 0 (Fig. 7B). The second constraint is that each cell is only optimally responsive over a narrow range of stimulus levels (roughly 20 dB) (Fig. 10C). This limitation, however, can easily be overcome if a population of cells are responsive to different "best" overall stimulus levels (as suggested by Fig. 10C).

In summary, AI response properties to rippled spectra suggest that it may function as a bank of ripple bandpass filters computing the local Fourier transform of the input spectral profile. For instance, a unit with a characteristic ripple frequency Ω_o and phase Φ_o would analyze the local region of the profile around its BF. More intuitively, the ripple frequency axis can be considered as a scale axis, with coarser views of the profile available at the low ripple filters, and finer details at the high ripple filters. Similarly, the ripple phase sensitivity axis can be seen as explicitly encoding the local asymmetry of the profile at each scale. The strength of its output reflects both the ripple frequency content near Ω_o, and the local asymmetry (relative to Φ_o) of that region of the profile. An array of such analyzers at different BFs, Ω_o's and Φ_o's would then perform the complete profile transformation.

The response nonlinearities and their implications

The correspondence observed between the various response measures using tonal and rippled stimuli suggests that threshold and saturation nonlinearities do not significantly disrupt the predominantly linear character of the responses. Linear response measures such as the ripple transfer function may indeed provide a meaningful characterization of a unit's response area. Perhaps the best way to explain this apparent paradox is by analogy to the effects of cochlear nonlinearities on the phase-locked responses of the auditory nerve.

For instance, the threshold nonlinearity of the cochlear hair cell rectifies the phase-locked responses of the auditory-nerve creating DC and higher harmonics that follow very similar trends as those described earlier in conjunction with Figs. 11 and 12 (Dallos and Santos-Sacchi 1983; Shamma et al. 1986). Thus, it is possible to measure on an auditory-nerve fiber an AC transfer function (analogous to $T(\Omega)$ in AI) based entirely on the phase-locked responses of the fiber using a swept single tone (Rose et al. 1971) or reverse-correlation techniques with a noise stimulus (de Boer and de Jongh 1978). Because of hair cell threshold, the synchronous responses are normally accompanied by a similarly tuned DC component (usually called the "average rate" response), much like the $DC(\Omega)$ component in AI responses (see Shamma et al. (1986) for a detailed discussion of these different response measures).

The saturation nonlinearity limits the growth of the ripple phase-locked responses in AI cells (Fig. 10) in an analogous manner to that seen in the synchronous responses on the auditory nerve. Note, however, that the decrease of $|T(\Omega)|$ at the highest stimulus levels is not analogously seen in auditory-nerve fibers (Rose et al. 1971) because they normally operate near the threshold knee of the nonlinear transfer characteristics of the hair cell and not near saturation.

Despite threshold and saturation nonlinearities, AC transfer functions on the auditory nerve are a valuable predictive measure of a fiber's response to broadband stimuli (Deng et al. 1988). It is in this sense that one may conjecture that ripple transfer functions $T(\Omega)$ are also useful in describing AI responses to a spectral profile.

A different source of nonlinear interactions is the uncertain "internal" representation of a

spectral ripple at the input of the central auditory system. Both linearly and logarithmically amplitude modulated rippled spectra were used as spectral profiles in our experiments. Clearly, one or both of these sinusoidal spectra may appear distorted to the central auditory system. This kind of "input nonlinearity" creates additional DC and higher harmonic components that are not explicitly accounted for in the stimulus. Nevertheless, the experimental results summarized in Fig. 8 suggest that the two inputs produce similar responses, suggesting that the distortion harmonics are smaller than the primary ripple and, for each unit, lie sufficiently away from its characteristic ripple (i.e., outside of the $|T(\Omega)|$).

All our experiments employed single ripples to measure the transfer functions $T(\Omega)$, i.e., analogous to measuring the cochlear bandpass filters with single tones. This leaves a fundamental question unanswered: do responses to multiple simultaneous ripples combine linearly? That is, in what sense and to what extent does the law of superposition hold in the hypothetical ripple analysis of AI? The answers to these questions have important implications both for the functional organization of AI and the peripheral representations of the acoustic spectrum. For instance, if superposition holds, then it must imply that it also holds at the cochlear outputs, and that the multitude of well known peripheral nonlinearities somehow do not destroy the linearity of the ripple analysis (Wang and Shamma 1994).

There are undoubtedly a host of other factors that affect the details of the responses, such as cell adaptation, anesthesia, and interactions among cells. For instance, the commonly observed double (and even triple) peaked transfer functions (Figs. 5A, 6B), may well reflect disinhibition associated with lateral inhibitory interactions among cells with different characteristic ripples, analogous to those observed in the visual cortex (De Valois and Tootell 1983). Also, it is possible that the depression of spontaneous activity caused by the anesthesia (Brugge and Merzenich 1973; Pfingst and O'Connor 1981) may exaggerate the effects of the threshold nonlinearity. All these factors and other previously discussed nonlinearities may induce their effects anywhere along the auditory pathway. In fact, the experiments here do not reveal the site of origin of any of the response features described in this paper since no similar physiological experiments using rippled spectra have been reported in pre-cortical structures.

Finally, a basic property of auditory-nerve responses is the loss of synchrony to high frequency tones (Palmer and Russell 1986), presumably due to the hair cell lowpass filter (Shamma et al. 1986). In this case, only (the nonlinear) DC or average rate tuning curve can be measured, and the responses are therefore insensitive to the phase of the tone. Analogously, in the ferret AI, there is a general decline in the number of cells tuned to higher ripple frequencies (Fig. 7A). This decline, however, is unlikely to be due to an analogous filtering of the ripple phase-locked responses since they can still be measured in some cells at ripples up to 4 cycles/octave (e.g., Fig. 9B). Furthermore, the decline does not seem to be compensated by an abundance of cells that are exclusively "$DC(\Omega)$ tuned" to higher ripples (> 1.5 cycles/octave) and are hence phase-insensitive. Instead, this narrow range of Ω_o's may reflect a genuine species-specific range of ripples to which the ferret is sensitive. And therefore, it is possible that in other species, there exists a broader range of characteristic ripples, or a large population of purely DC-tuned, phase-insensitive cells. In fact, this distinction between ripple phase-sensitive (linear) and ripple phase-insensitive (nonlinear) cells is identical to the distinction between simple (linear) and complex (nonlinear) cells of the visual cortex (Hubel and Wiesel 1962; De Valois et al. 1982).

Relation to spatial frequency analysis in the visual cortex

Physiological and psychophysical experiments with ripple-like stimuli (or gratings) in the visual system have been carried out for over two decades (see De Valois and De Valois (1988) for a thorough review). In the primary visual cortex (VI), cells display similar responses to those described here in AI. For instance, the transfer function of a VI cell is tuned around a specific grating frequency (usually called "spatial frequency"), and its inverse transform predicts well the receptive field of the cell measured by impulse-like stimuli as light dots (De Valois et al. 1982). Thus, just as in AI, visual cortical responses have a substantial linear component that is not disrupted by threshold, saturation, and other nonlinearities. Furthermore, psychophysical data has accumulated in the visual literature that supports the notion that these tuned response features are perceptually relevant (De Valois and De Valois 1988).

Ripple (or grating) phase has played only a secondary role in most physiological experiments of spatial frequency selectivity in VI. Nevertheless, it has served to distinguish cleanly between two fundamental classes of cortical cells, simple and complex cells, long recognized by a variety of other criteria (Hubel and Wiesel 1962). Thus, while both cell types have tuned transfer function magnitudes, only simple cells exhibit clear phase-locked responses. The distributions of these two cell types in VI are basically comparable (De Valois and De Valois 1988). By contrast, there are very few units that can be analogously called "complex cells" in the ferret AI as most exhibit robust "linear" sensitivity to the phase of the ripple.

Another significant difference between the responses of AI and VI with respect to ripple phase sensitivity concerns the relative dearth in our AI sample of units with "reverse" RFs, i.e., with $|\phi_o| > 150$ (as in Fig. 14B). Such RFs in VI (known as off-center-on-surround) are at least as common as their counterparts. It is possible they were missed in AI due to a bias in the sampling procedures, or are concentrated in sub-areas of AI as yet undiscovered in the ferret. For instance, such cells (exhibiting doubly-tuned excitatory response areas) have been reported to be concentrated in the dorsal area of AI in the cat (Sutter and Schreiner 1991).

Finally, it is possible to give a simple interpretation of orientation selectivity in VI within the context of spatial frequency analysis, and relate it to ripple analysis in AI. Visual gratings are two-dimensional in nature with "spatial frequencies" defined along two axes of a scene (e.g, Ω_x and Ω_y). Oriented gratings can be uniquely defined (within a quadrant) by a combination of these two spatial frequencies. For instance, vertical (horizontal) gratings are those with $\Omega_y = 0$ ($\Omega_x = 0$), while those with equal spatial frequencies ($\Omega_x = \Omega_y$) correspond gratings oriented at 45°. Thus, VI cells (simple or complex) tuned to different spatial frequency combinations would exhibit orientation selectivity. Since spectral ripples are one-dimensional, "orientation selectivity" as defined above simply reduces to tuning along one dimension, i.e., the usual characteristic ripple (Ω_o). However, it is crucial to recognize that apart from the dimensionality of the input signal, the mechanisms giving rise to orientation selectivity in VI are identical to those seen in AI.

Relation to psychoacoustics

We suggested so far that a spectral profile of an acoustic stimulus is analyzed by AI filters, each operating locally on the tonotopic axis and each filtering both ripple frequencies to encode the profile scale and ripple phases to encode the profile asymmetry. There are many psychoacoustical implications of this hypothesis, but very few experiments have been carried

out so far to test them. One of the earliest studies by Green (1986), and a recent more detailed elaboration on it by Hillier (1991), tested the sensitivity of human subjects to rippled spectra of different frequencies. They both found increased sensitivity and uniformity of thresholds around approximately 1-3 cycles/octave; nevertheless, subjects responded over a broad range of ripples well exceeding 10 cycles/octave. Similarly, recent measurements (Vranić-Sowers and Shamma 1994a) revealed that ripple phase sensitivity up to approximately 1 cycle/octave is constant at around 6° regardless of ripple frequency. Above 1 cycle/octave, threshold increased gradually. These thresholds values and trends are almost identical to those found in corresponding visual experiments (De Valois and De Valois 1988).

In summary, it is hypothesized that the auditory system analyzes locally the spectral profile along a ripple frequency (scale) and a phase (asymmetry) dimension (Vranić-Sowers and Shamma 1994b). An implication of this hypothesis is that the perception of timbre (as far as determined by the shape of the spectral profile) may be more accurately described using the ripple analyzed profile, rather than the profile itself. Similarly, and more generally, descriptions of higher level auditory perceptual tasks involving complex sounds, such as spatial localization, pitch perception, speech recognition, and detection of spatial and spectral motion, should be based upon an explicit representation of the ripple transformation of the spectral profile.

ACKNOWLEDGEMENTS

REFERENCES

BILSEN, F. A., TEN KATE, J. H., BUUNEN, F. AND RAATGEVER, J. Response of single units in the cochlear nucleus of the cat to cosine noise. *J. Acoust. Soc. Am.* 58: 858-866, 1975.

BRUGGE, J. F. AND MERZENICH, M. M. Responses of neurons in auditory cortex of the Macaque monkey to monaural and binaural stimulation. *J. Neurophysiol.* 36: 1138-1158, 1973.

CALHOUN, B. M. AND SCHREINER, C. E. Spatial frequency filters in cat auditory cortex (Abstract). *Soc. Neurosci.*, Washington, D.C., 1993.

DALLOS, P. AND SANTOS-SACCHI, J. AC Receptor potentials from hair cells in the low-frequency region of the guinea pig cochlea. In: *Mechanisms of Hearing* edited by W.R. Webster and L.M. Aitkin. Australia: Monash University Press, 1983, p. 11-16.

DE BOER, E. AND DE JONGH, H. R. On cochlear encoding: Potentialities and limitations of the reverse-correlation technique. *J. Acoust. Soc. Am.* 63: 115-135, 1978.

DENG, L., GEISLER, C. D. AND GREENBERG, S. A composite model of the auditory periphery for the processing of speech. *J. Phonetics.* 16: 1988.

DE VALOIS, K. AND TOOTELL, R. B. H. Spatial-frequency-specific inhibition in cat striate cortex cells. *J. Physiol. Lond.* 336: 359-376, 1983.

DE VALOIS, R., ALBRECHT, D. G. AND THORELL, L. G. Spatial frequency selectivity of cells in macaque visual cortex. *Vision Res.* 22: 545-559, 1982.

DE VALOIS, R. AND DE VALOIS, K. *Spatial Vision.* New York: Oxford University Press, 1988.

EVANS, E. F. Single-unit studies of mammalian cochlear nerve. In: *Auditory investigation: The technological and scientific basis* edited by H. A. Beagley. Oxford: Clarendon Press: 1979, p. 324-367.

GREEN, D. M. 'Frequency' and the detection of spectral shape change. In: *Auditory Frequency Selectivity* edited by B. C. J. Moore and R. D. Patterson. Cambridge: Plenum Press, 1986, p. 351-359.

HEIL, P., RAJAN, R. AND IRVINE, D. Sensitivity of neurons in cat primary auditory cortex to tones and frequency-modulated stimuli. II. Organization of response properties along the iso-frequency dimension. *Hear. Res.* 63: 135-156, 1992.

HILLIER, D. Auditory processing of sinusoidal spectral envelopes. Doctoral thesis, Washington University, St. Louis, 1991.

HUBEL, D. AND WIESEL, T. Receptive Fields and functional architecture of monkey striate cortex. *J. Physiol. Lond.* 195: 215-243, 1968.

KIANG, N. Y. S., WATANABE, T., THOMAS, E. C. AND CLARK, L. F. *Discharge patterns of single fibers in the cat's auditory nerve.* M.I.T. Research Monograph No.35, Cambridge: M.I.T. Press, 1965.

NELKEN, I., PRUT, Y., VAADIA, E. AND ABELES, M. Population responses to multifrequency sounds in the cat auditory cortex: One- and two-parameter families of sounds. *Hear. Res.* 72: 206-222, 1994.

OPPENHEIM, A. AND SCHAFER, R. *Digital Signal Processing.* New Jersey: Prentice-Hall, 1990.

PALMER, A. R. AND RUSSELL, I. J. Phase-locking in the cochlear nerve of the guinea-pig and its relation to the receptor potential of inner hair-cells. *Hear. Res.* 24: 1-15, 1986.

PFEIFFER, R. R. AND KIM, D. O. Response patterns of cochlear nerve fibers to click stimuli: descriptions for cat. *J. Acoust. Soc. Am.* 52: 1669-1677, 1972.

PFINGST, B. E. AND O'CONNOR, T. A. Characteristics of neurons in auditory cortex of monkeys performing a simple auditory task. *J. Neurophysiol.* 45: 16-34, 1981.

PICKLES, J. O. The neurophysiological basis of frequency selectivity. In: *Frequency Selectivity in Hearing* edited by B. C. J. Moore. London: Acadamic Press, 1986, p. 51-122.

ROSE, J. E., HIND, J. E., ANDERSON, D. J. AND BRUGGE, J. F. Some effects of stimulus intensity on response of auditory nerve fibers of the squirrel monkey. *J. Neurophysiol.* 34: 685-699, 1971.

SCHREINER, C. E. AND MENDELSON, J. R. Functional topography of cat primary auditory cortex: distribution of integrated excitation. *J. Neurophysiol.* 64: 1442-1459, 1990.

SHAMMA, S. A. FLESHMAN, J. W., WISER, P.R. AND VERSNEL, H. Organization of response areas in ferret primary auditory cortex. *J. Neurophysiol.* 69: 367-383, 1993.

SHAMMA, S. A., CHADWICK, R. S., WILBUR, W. J., MORRISH, K. A. AND RINZEL, J. A biophysical model of cochlear processing: intensity dependence of pure tone responses. *J. Acoust. Soc. Am.* 80: 133-145, 1986.

SUTTER, M. L. AND SCHREINER, C. E. Physiology and topography of neurons with multipeaked tuning curves in cat primary auditory cortex. *J. Neurophysiol.* 65: 1207-1226, 1991.

VERSNEL, H., KOWALSKI, N. AND SHAMMA, S. A. Ripple analysis in the ferret primary auditory cortex. II. Topographic distribution of ripple response parameters. *ISR Technical Report 94-21, University of Maryland, College Park, 1994.*

VRANIC', S., VERSNEL, H. AND SHAMMA, S. A. Single and double spectral peaks: psychoacoustical and physiological results (Abstract). *ARO,* St. Petersburg, 1993.

VRANIC'-SOWERS, S. AND SHAMMA, S. A. Representation of spectral profiles in the auditory system. II. Detection of spectral peak shape changes. *ISR Technical Report 94-15, University of Maryland, College Park, 1994a.*

VRANIC'-SOWERS, S. AND SHAMMA, S. A. Representation of spectral profiles in the auditory system. I. A ripple analysis model. *ISR Technical Report 94-14, University of Maryland, College Park, 1994b.*

WANG, K. AND SHAMMA, S. A. Self-normalization and noise robustness in auditory representations. *IEEE Trans. Audio. Speech. Proc.* 2: (in press), 1994.

YOST, W. A., HILL, R. AND PEREZ-FALCON, T. Pitch and pitch discrimination in broadband signals with rippled power spectra. *J. Acoust. Soc. Am.* 63: 1166-1173, 1978.

Figure Legends

FIG. 1. Scheme of presumed responses of an array of AI cells uniformly distributed along the tonotopic axis. *A*: The responses to a single tone. The tone is represented by an impulse stimulus along the tonotopic axis. The tone evokes a pattern of cells' responses along the axis that mirrors the typical response area of a single cell with its excitatory tuned center and inhibitory sidebands (shaded region). The pattern is slightly asymmetric, thus reflecting asymmetric response areas of the array's cells. *B*: The response pattern evoked by a rippled spectrum stimulus. The stimulus is represented by a sinusoid along the tonotopic axis. The output is an alternating (sinusoidal) pattern of excitation and inhibition, that is amplified or attenuated in amplitude, and phase-shifted relative to the input pattern. A transfer function can be measured by noting the amplitude and phase of the output relative to the input ripple at various ripple frequencies. As in *A*, the cells in this scheme have asymmetric response areas reflected here by a phase shift.

FIG. 2. Scheme of a rippled spectrum stimulus. It is composed of 101 tones equally spaced along the logarithmic frequency axis between 1-20 kHz. The envelope is sinusoidally modulated on either a linear (left ordinate) or a logarithmic (right ordinate) amplitude scale. The ripple phase is defined relative to a sinewave starting at the left edge. For the ripple shown, the amplitude (ΔA) is either 50% (linear) or 10 dB (logarithmic), the ripple frequency $\Omega = 0.5$ cycles/octave, and the ripple phase $\Phi = 90°$.

FIG. 3. The analysis of the responses to rippled stimuli. *A*: Raster of the responses of an AI cell (#148/06c; BF of 7.5 kHz) to a rippled spectrum stimulus ($\Omega = 0.8$ cycles/octave) at various ripple phases ($0° - 315°$ in steps of $45°$). The stimulus burst starts at 100 ms and lasts for 50 ms. Stimulus is repeated 20 times for each ripple phase. Spike counts as a function of the ripple are computed over a 50 ms window as indicated by the bold arrows, and are displayed in the inset plot to the right of the raster. *B*: Spike counts as a function of ripple phase for various ripple frequencies Ω between 0 and 2 cycles/octave. At each Ω, spike counts are indicated by the circles, and the abscissa is placed at the spike count averaged over all phases. The solid line is the best sinusoidal fit to the points (in the sense of mean square error). *C*: An 8-point Fourier transform of the spike counts at each Ω yields estimates of the average spike count, $DC(\Omega)$, and the amplitude and phase of the best sinusoidal fit, $AC_1(\Omega)$, and of the 2nd, 3rd, and 4th (distortion) harmonics of the fundamental (Ω).

FIG. 4. The transfer function and the response field. *A*: The transfer function $T(\Omega)$ derived from the responses in Fig. 2. Plot to the left is of the $|AC_1(\Omega)|$, the magnitude of the fundamental component of the Fourier analysis in Fig. 2C. $|T(\Omega)|$ is a normalized version of $|AC_1(\Omega)|$. The characteristic ripple Ω_o is the location of the maximum of $|T(\Omega)|$. Plot to the right depicts the phase function $\Phi(\Omega)$ (filled circles) of the fundamental component $AC_1(\Omega)$ (or of the transfer function $T(\Omega)$). The solid line represents a linear fit to the data with intercept Φ_o and slope x_o. *B*: The response field (RF) of the cell derived by an inverse Fourier transform of the transfer function $T(\Omega)$. The dashed curve represents the envelope of the RF. The distance from the left edge of the rippled spectrum to the center of the RF envelope is equal to the slope x_o in $\Phi(\Omega)$ (see *A*). The location of the maximum of the RF is defined as BF_{RF}. *C*: Several RFs derived

from the same $|T(\Omega)|$ and x_o as in A, but with different Φ_o's. Changing the Φ_o's results in RFs of different asymmetries.

FIG. 5. Examples of ripple responses from three cells (A, B, C) with different characteristic ripples (Ω_o = 0.6, 1.0, 2.0 cycles/octave, respectively), but similar asymmetries (Φ_o = $-10°, 17°, -11°$). For each cell, the left plot depicts the magnitude of its ripple transfer function $|T(\Omega)|$. Data points are connected by straight line segments, and are then smoothed by linearly interpolating the slopes between the midpoints of adjacent segments. The middle plot represents the phase function $\Phi(\Omega)$, and the linear fit to the data points. The phase-fit indicators for the three cells are 0.99, 1.00, and 0.99. The right plot illustrates the corresponding RF.

FIG. 6. Examples of ripple responses from three cells (A, B, C) with different characteristic phases (Φ_o = $-106°, 7°, 53°$, respectively), but similar characteristic ripples (Ω_o = 0.8 − 1.0 cycles/octave). Other details of the plots are as in Fig. 5. The phase-fit indicators for the three cells are 0.98, 0.98, 0.93.

FIG. 7. Distributions of ripple response parameters in single-unit recordings in AI. A: Distribution of characteristic ripple Ω_o. B: Distribution of characteristic phase Φ_o. C: Distribution of Ω_o as a function of BF. The solid line represents the linear regression, which indicates a weak but significant correlation ($r = 0.25$, $P < 0.05$). D: Distribution of Φ_o as a function of BF. E: Combined distribution of Ω_o and Φ_o. At four intervals of Ω_o (0-0.6; 0.6-1.2; 1.2-1.8; > 1.8) the means and SD of Φ_o were computed; the dashed lines represent a smoothed connection of the 2SD edges.

FIG. 8. Examples of ripple responses from two cells (A, B) with rippled inputs defined on a logarithmic (solid line, open circle) or linear (dashed line, filled circle) amplitude scale. Organization and symbols of the plots are as in Fig. 5. The phase-fit indicators for the two cells both are 1.00.

FIG. 9. Examples of ripple responses from two cells (A, B) for various ripple amplitudes. For both cases three ripple amplitudes were presented as indicated in the bottom legend. The ripples are defined on a linear amplitude scale in (A), and a logarithmic scale in (B). Organization and symbols of the plots are as in Fig. 5. The phase-fit indicators for the unit in (A) at the three ripple amplitudes (in decending order) are 0.99, 0.99, and 0.98. The phase-fit indicators for the unit in (B) are 0.87, 0.89, and 0.74.

FIG. 10. Examples of ripple responses as a function of overall level of the stimulus. Plots in A and B are organized as in Fig. 5. A: A nonmonotonic unit tested at three stimulus levels. B: A monotonic unit tested at two stimulus levels. C: Response magnitude at the characteristic ripple, $|T(\Omega = \Omega_o)|$, as a function of overall stimulus level for three cells.

FIG. 11. The effects of nonlinearities on the ripple responses of a non- monotonic cell. A: The nonmonotonic rate-level function of the cell measured with a single tone at BF (8.5 kHz). B: Responses as a function of ripple phase at $\Omega = 0.4$ cycles/octave, at two overall levels. Details as in Fig. 3B. C: Magnitude of ripple transfer functions at levels as in B. Details as in Fig. 4A.

D: The $DC(\Omega)$ component of the response at levels as in *B*. The responses are computed as shown in Fig. 2*C*. Note that the trend of response decrease with increase of level, is similar as in *C*.

FIG. 12. The effects of the nonlinearities on the ripple responses of a monotonic cell. All plots as in Fig. 11. Plots *B, C* and *D* for two different overall stimulus levels. *A*: The rate-level function at a BF tone of 2.0 kHz. *B*: The phase-locked responses at $\Omega = 1.5$ cycles/octave. *C*: Magnitude of ripple transfer functions. *D*: The $DC(\Omega)$ response. Note that the trends of $AC(\Omega)$ and $DC(\Omega)$ responses level are opposite.

FIG. 13. Magnitude of ripple transfer function $|T(\Omega)|$ (*top*) and the $DC(\Omega)$ responses (*bottom*) of a more complex cell. Plots as in Fig. 4*A* and Fig. 3*B*, respectively. The two curves are uncorrelated to each other. The $DC(\Omega)$ is tuned at high ripple frequencies (4 - 7 cycles/octave) whereas the AC component is tuned to a low ripple frequency (0.4 cycles/octave).

FIG. 14. Comparison between tonal response areas and ripple response fields (RFs). *A*: Examples of responses from three cells. The response areas (dashed lines) are measured using the two-tone paradigm, and hence the response counts are artificially elevated towards the edges (cf. Shamma et al. 1993). The RFs and response areas exhibit similar bandwidths, asymmetries, and BFs. *B*: An atypical example of a cell with both RF and excitatory response area double tuned.

FIG. 15. Scatter plot comparing the BF measured with a single tone (abscissa) to the BF_{RF} predicted from the ripple responses (ordinate). The solid line represents the $BF_{RF} = BF$ line and the dashed lines represent the half-octave deviations. In only 7 cases the deviations are half of an octave or larger.

FIG. 16. Ripple response measures compared to the bandwidth of the response areas. The solid lines represent linear regression lines. Correlation measures are indicated in the right-hand corner. In both plots only cells with $|\Phi_o| < 90^\circ$ are used. *A*: The width of the RF versus the bandwidth of the response area, BW20. *B*: The characteristic ripple Ω_o versus BW20.

FIG. 17. The asymmetry of the RF reflected by characteristic ripple phase compared to tonal measures. Only cells with $|\Phi_o| < 90^\circ$ are used. *A*: The characteristic phase Φ_o versus the response area asymmetry, *M* index. *B*: The characteristic phase Φ_o versus FM direction sensitivity, *C* index. *C*: Scatter plot between *C* index and *M* index.

A

Output Impulse Response
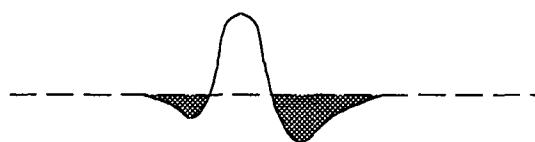
Neural Array

Input Tone Spectrum
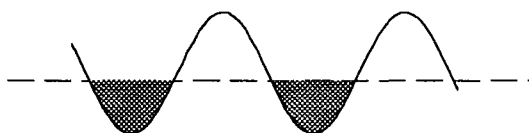
Spontaneous activity level

Tonotopic axis (low → high)

B

Output Ripple

Neural Array

Input Ripple Spectrum

Spontaneous activity level
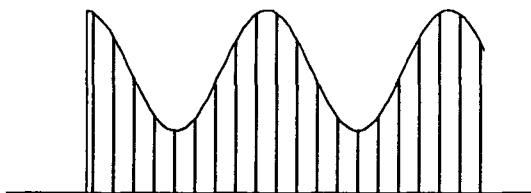
Tonotopic Axis (low → high)

Figure 1

Figure 2

A

148/06c

Phase (deg)

0

90

180

270

Time (ms)
0   100   200

Spike Count

10   20

10   20

$\Omega = 0.8$
cycles/octave

Stimulus

B

Spike Count

$\Omega = 0.0$

$\Omega = 0.4$

$\Omega = 0.8$

$\Omega = 1.2$

$\Omega = 1.6$

$\Omega = 2.0$

Ripple Phase (degrees)
0   45   90   135   180   225   270   315   360

C
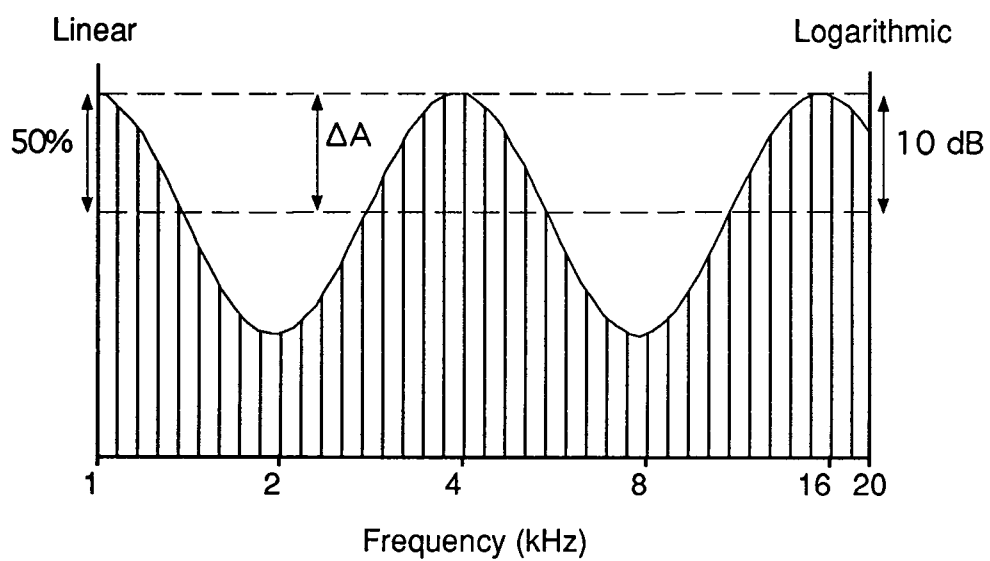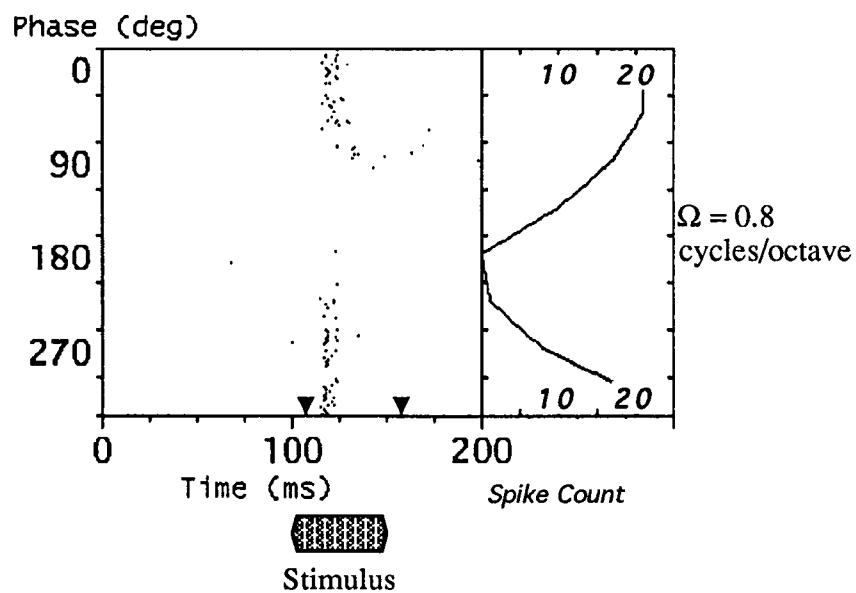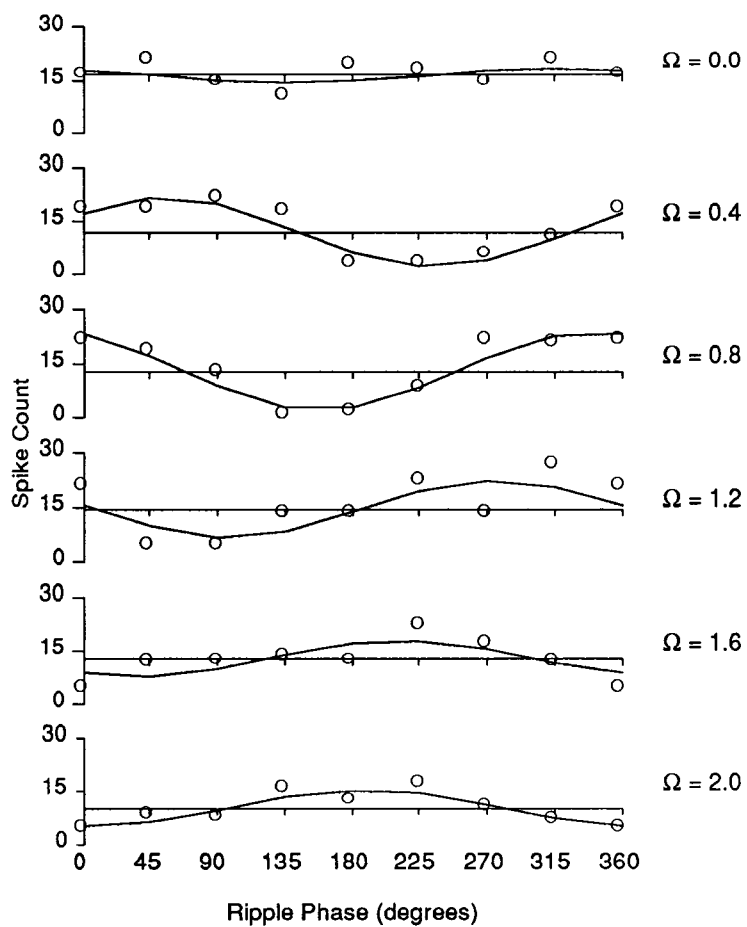
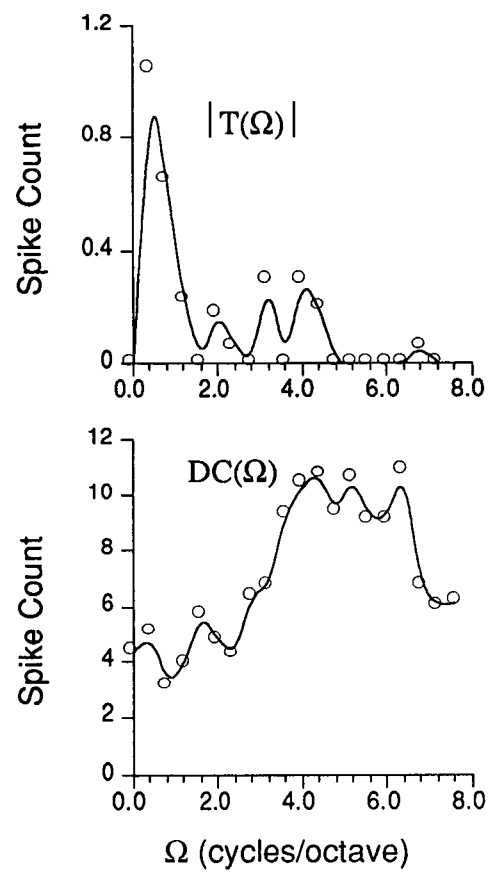| Ω	$DC(\Omega)$	$AC_1(\Omega)$	$AC_2(\Omega)$	$AC_3(\Omega)$	$AC_4(\Omega)$
0.0	16.25	1.98 129°	2.47 45°	3.29 -112°	1.00 -90°
0.4	11.62	9.81 30°	2.30 -139°	2.41 88°	0.25 -90°
0.8	12.62	11.06 111°	3.13 -61°	0.57 -32°	2.25 90°
1.2	14.38	7.78 174°	5.15 129°	4.17 141°	3.75 -90°
1.6	12.75	5.15 -124°	3.95 -55°	0.45 139°	3.00 -90°
2.0	9.88	5.24 -98°	1.03 -14°	1.40 58°	3.25 -90°

Figure 3
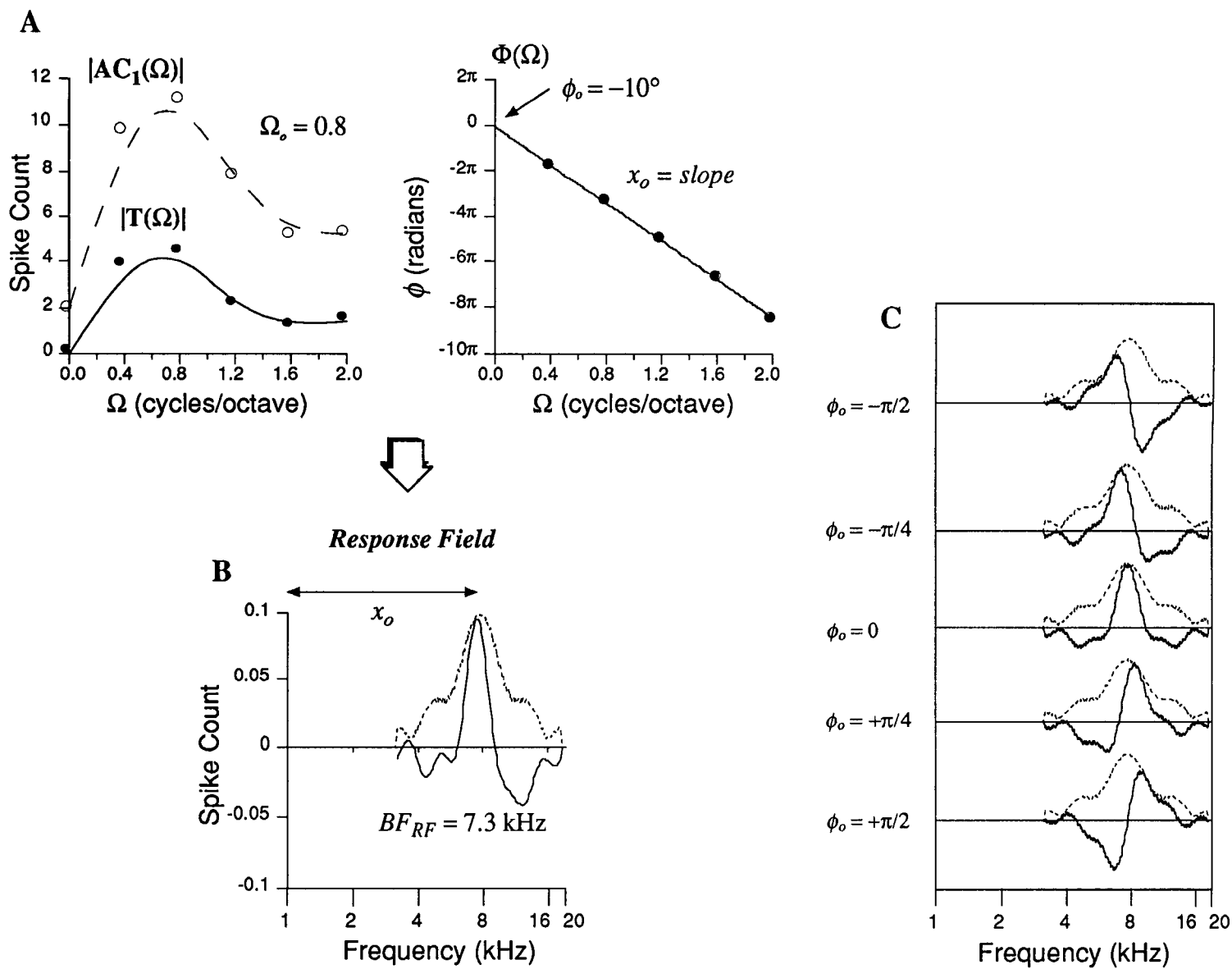
Figure 4
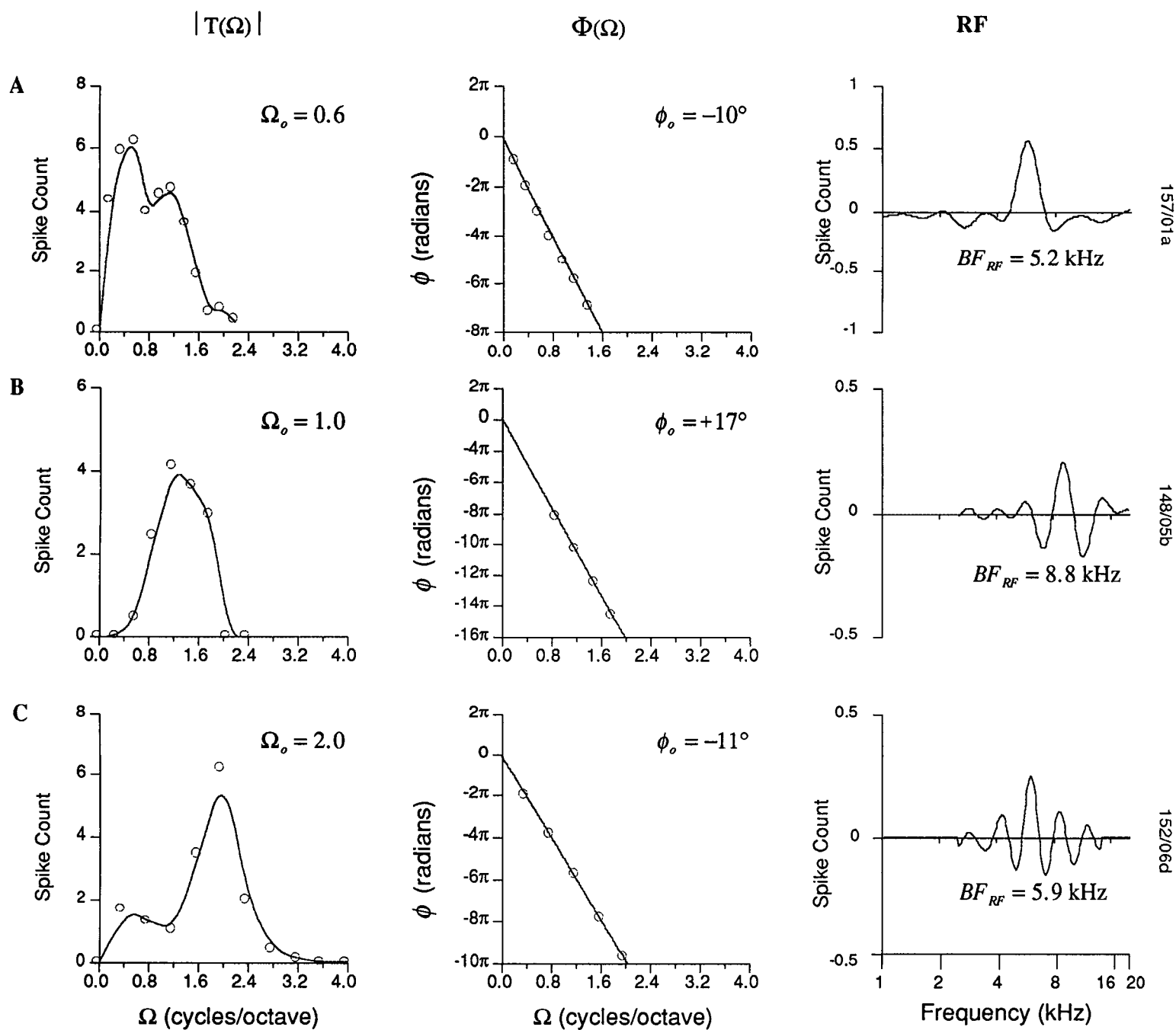
Figure 5
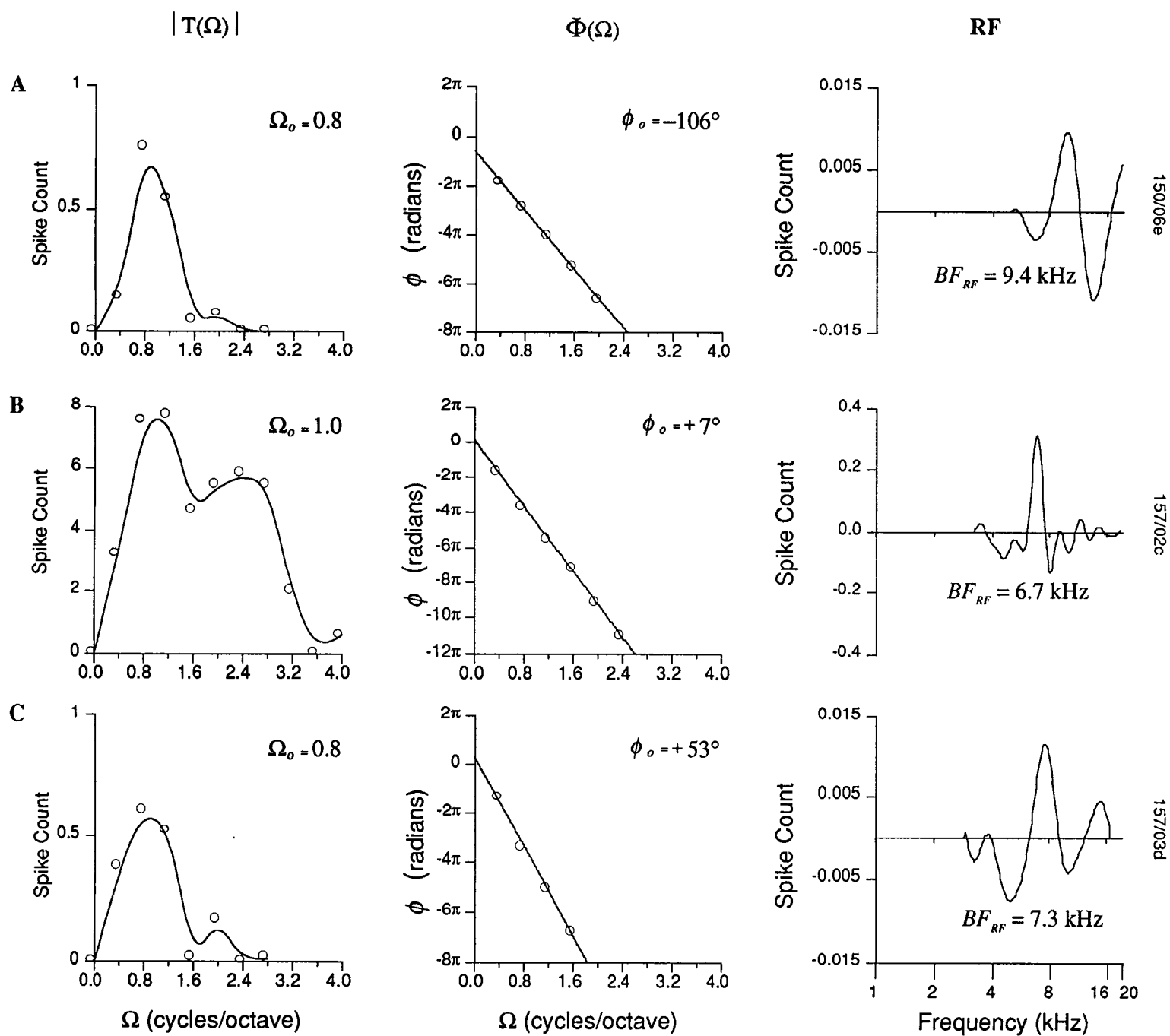
Figure 6
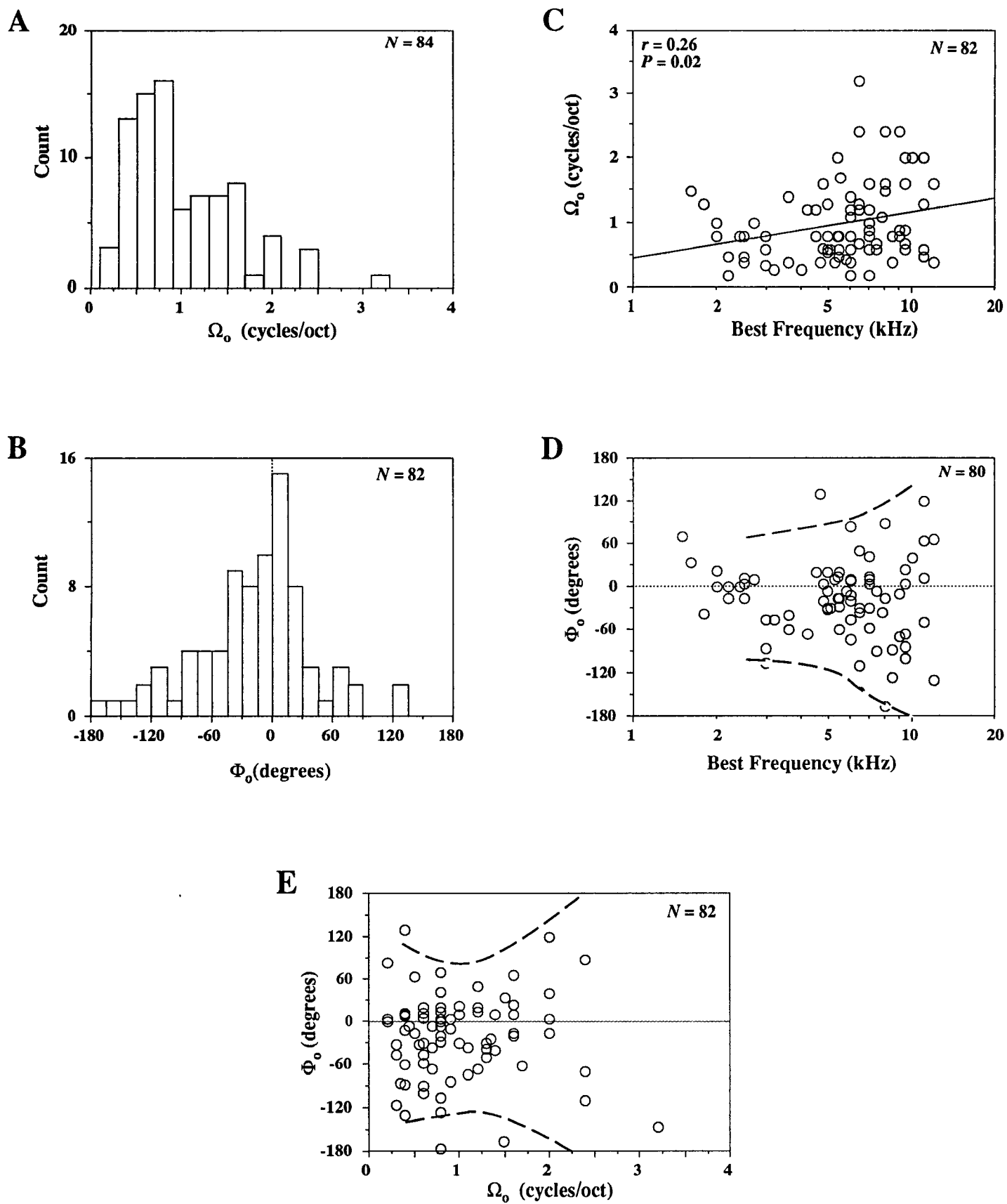
Figure 7
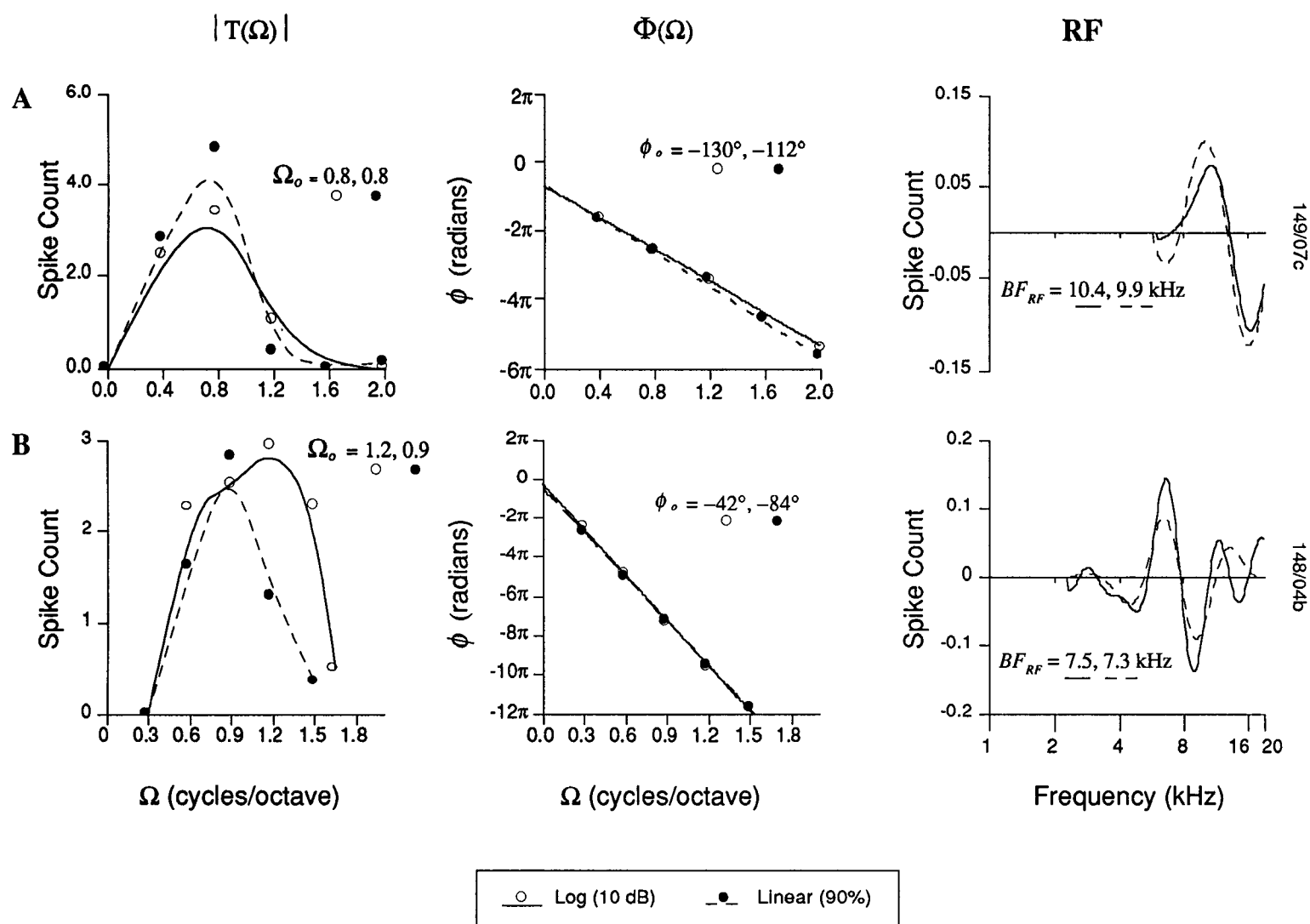
Figure 8

Figure 9

Figure 10

A

B

$\Omega = 0.4$

C

$|T(\Omega)|$

$\Omega_o = 0.8, 0.8$

D

$DC(\Omega)$

Ω (cycles/octave)

○ ___ 50 dB   ● - - - 60 dB
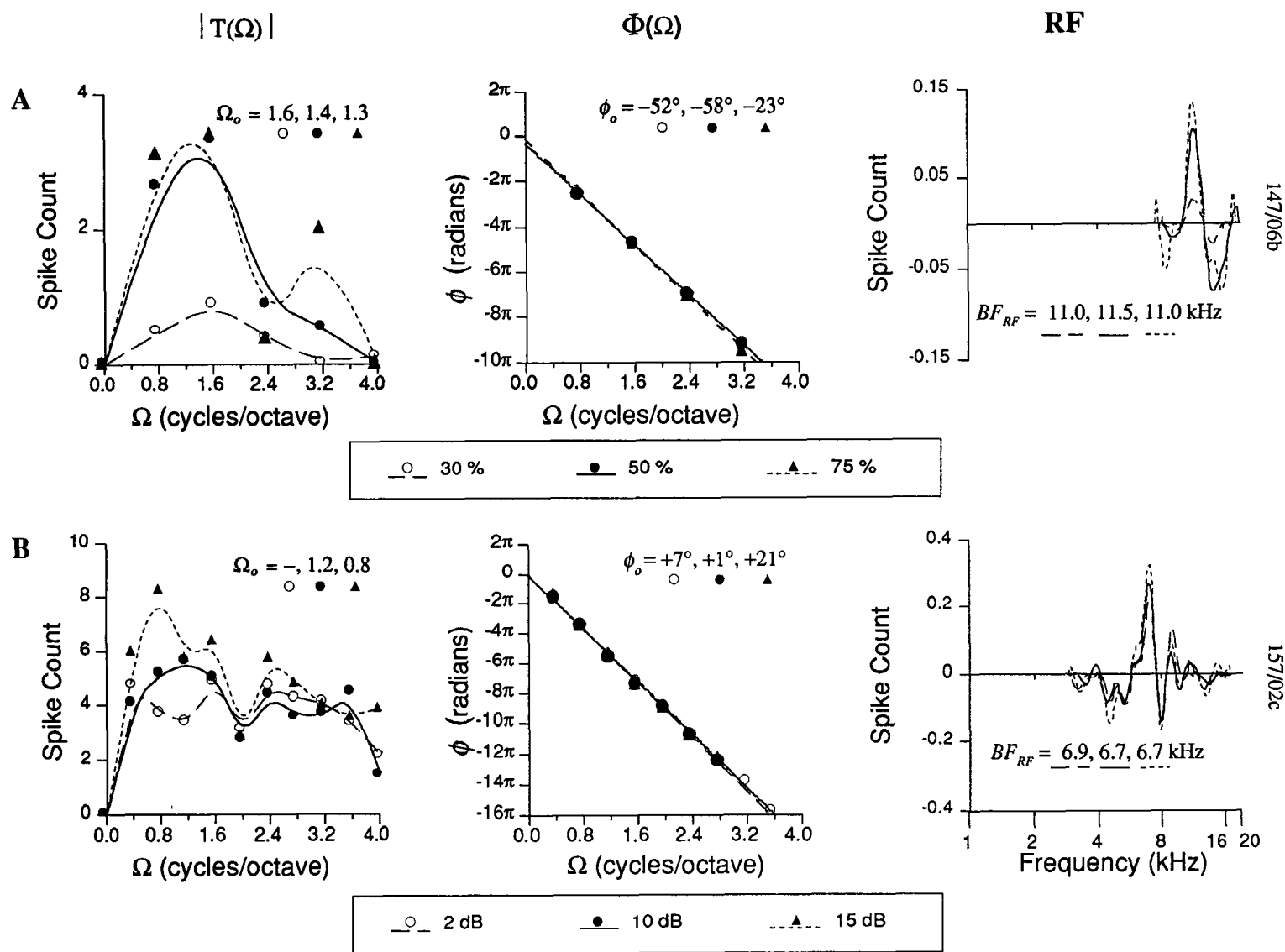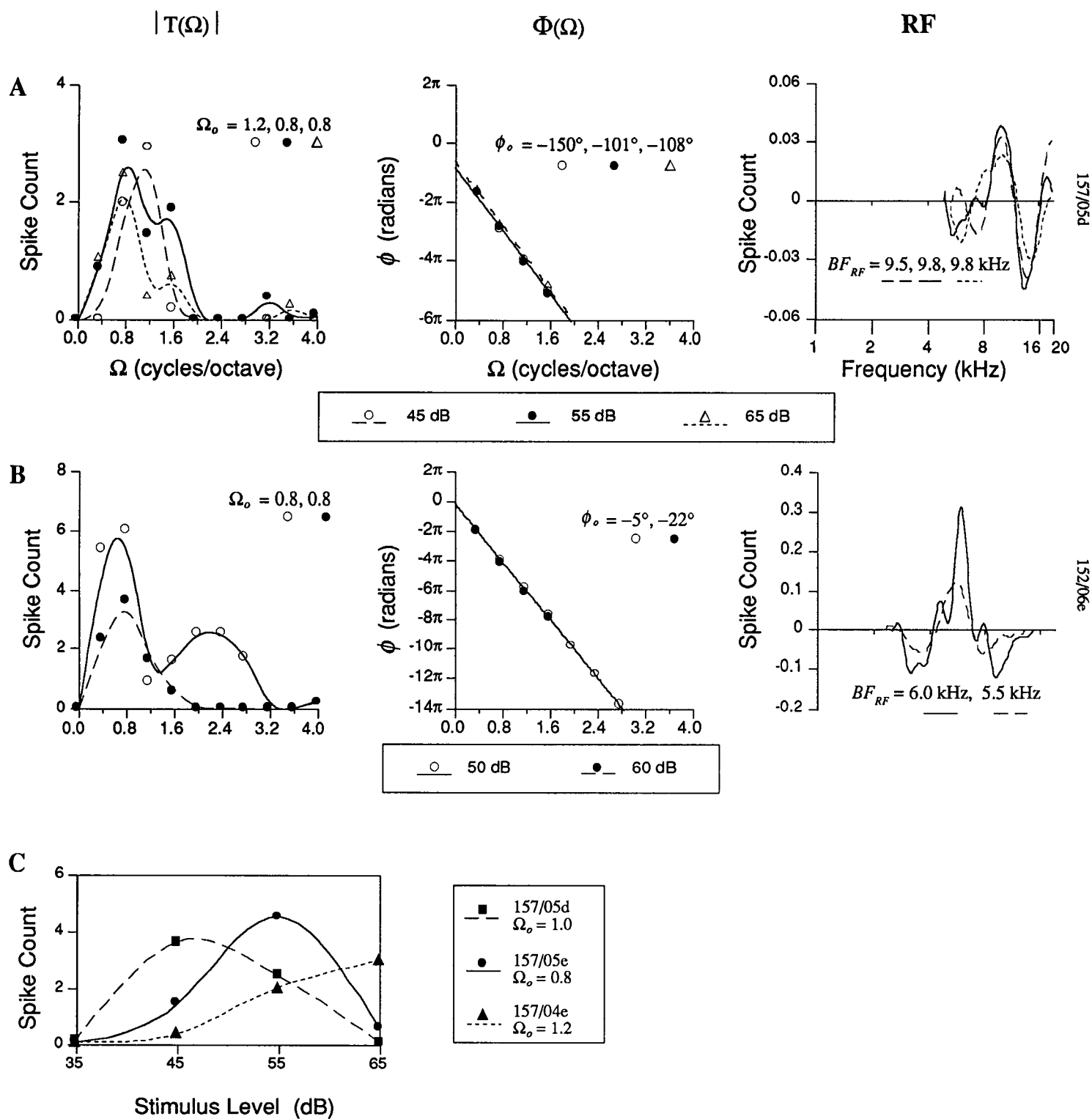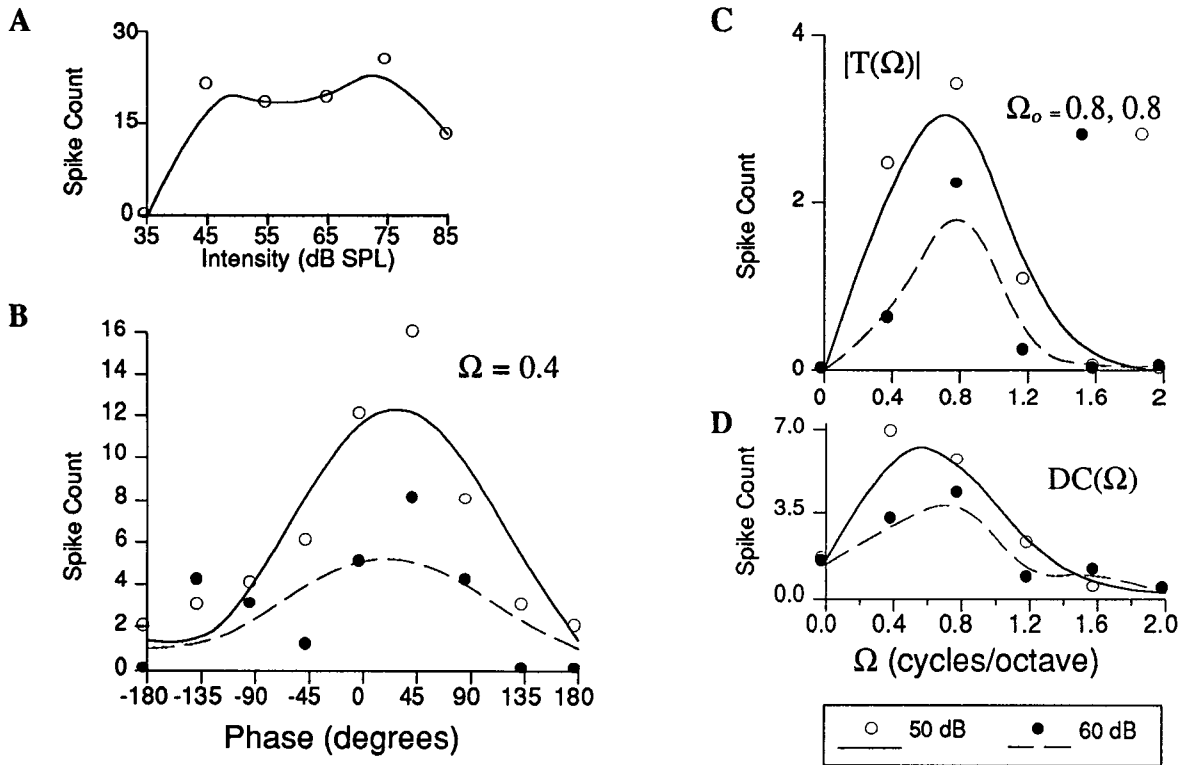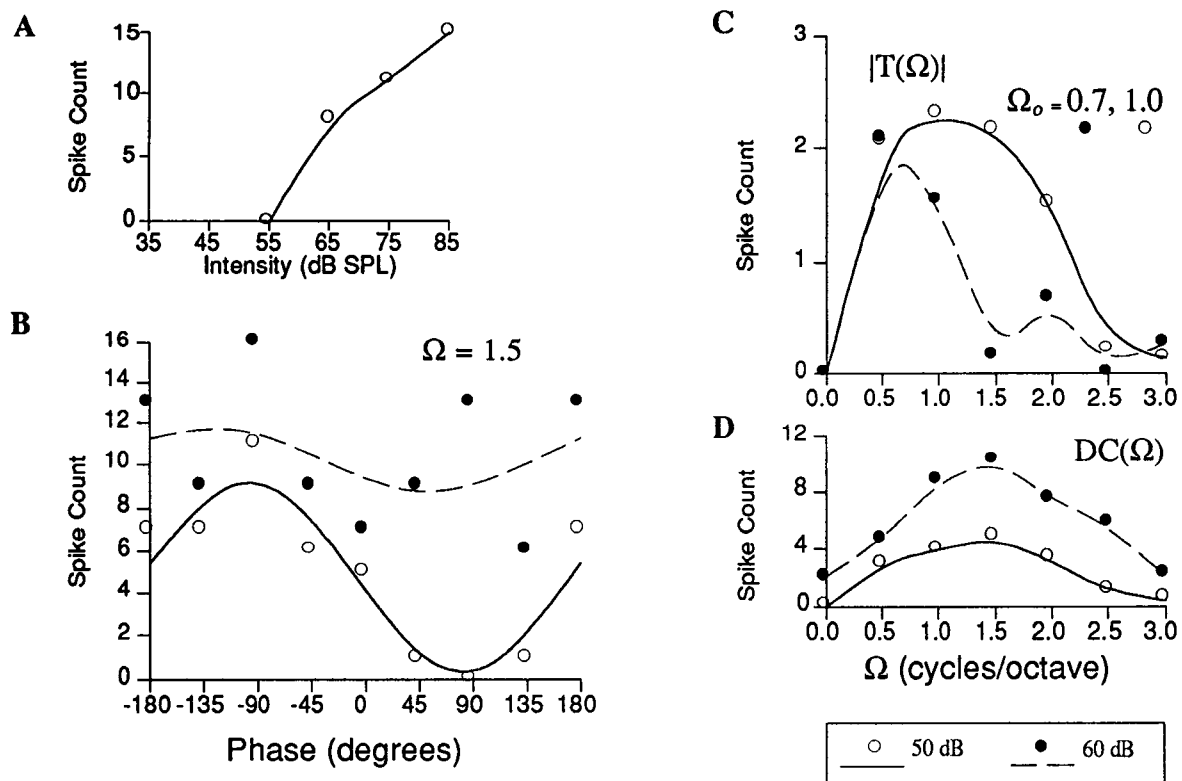
Figure 11

Figure 12

Figure 13

Figure 14

Figure 15

A

Graph A: RF Width (oct) versus BW20 (oct), with $|\phi_o| < 90°$, $N = 67$, $r = 0.32$, $P = 0.007$

B

Graph B: Ω_o (cycles/oct) versus BW20 (oct), with $|\phi_o| < 90°$, $N = 67$, $r = -0.29$, $P = 0.02$

Figure 16

Figure 17